3

THE LUNAR ENVIRONMENT

David Vaniman, Robert Reedy, Grant Heiken, Gary Olhoeft, and Wendell Mendell

3.1. EARTH AND MOON COMPARED

The differences between the Earth and Moon appear clearly in comparisons of their physical characteristics (Table 3.1). The Moon is indeed an alien environment. While these differences may appear to be of only academic interest, as a measure of the Moon's "abnormality," it is important to keep in mind that some of the differences also provide unique opportunities for using the lunar environment and its resources in future space exploration.

Despite these differences, there are strong bonds between the Earth and Moon. Tidal resonance between Earth and Moon locks the Moon's rotation with one face (the "nearside") always toward Earth, the other (the "farside") always hidden from Earth. The lunar farside is therefore totally shielded from the Earth's electromagnetic noise and is—electromagnetically at least—probably the quietest location in our part of the solar system. The Moon has also been moving away from Earth over time, because the dissipation of tidal energy by bottom friction in the Earth's seas (especially in shallow seas) has gradually slowed the Earth's rotation (e.g., *Lambeck,* 1975). To keep the angular momentum of the Earth-Moon system constant, the Moon has been moving slowly outward at a rate of a few centimeters per year.

The relationships between the Earth and Moon in origin, composition, and orbital dynamics are as important for the basing of people and equipment on the Moon as they are for scientific understanding. However, in considering routine terrestrial processes transplanted to the Moon, it is primarily the many differences in Table 3.1 that stand out.

On the Moon the most obvious environmental factors that concern people are extreme temperature fluctuations, low gravity, and the virtual absence of any atmosphere. Other environmental factors are not so evident. Of these the most important is ionizing radiation, and much of this chapter is devoted to the details of solar and cosmic radiation that constantly bombard the Moon. Of lesser importance, but necessary to evaluate, are the hazards from micrometeoroid bombardment, the nuisance of electrostatically charged lunar dust, and alien lighting conditions without familiar visual clues. To introduce these problems, it is appropriate to begin with a human viewpoint—the Apollo astronauts' impressions of environmental factors that govern the sensations of working on the Moon.

3.2. THE ASTRONAUT EXPERIENCE

Working within a self-contained spacesuit is a requirement for both survival and personal mobility on the Moon. Spacesuits overcome the extreme lunar temperatures and the lack of air, and they are adequately mobile (although awkward) in the low gravity. Current technology in spacesuit design provides for survival but is far from the optimum in comfort. Spacesuits used on the Apollo missions were bulky; maneuvering in the awkward suits was compensated for by low lunar gravity, so that mobility on the Moon was not much different from mobility on Earth without a suit. The Apollo 11 astronauts remarked that "the lunar gravity field . . . has differing effects on Earth-learned skills. Although the gravitational pull on the Moon is known to be one-sixth of the gravitational pull on the Earth, objects seem to weigh approximately one-tenth of their Earth weight. [Objects are] easy to

TABLE 3.1. Physical comparison of the Moon and Earth.

Property	Moon	Earth
Mass	7.353×10^{22} kg	5.976×10^{24} kg
Radius (spherical)	1738 km	6371 km
Surface area	37.9×10^{6} km^2	510.1×10^{6} km^2 (land = 149.8×10^{6} km^2)
Flattening*	0.0005	0.0034
Mean density	3.34 g/cm^3	5.517 g/cm^3
Gravity at equator	1.62 m/sec^2	9.81 m/sec^2
Escape velocity at equator	2.38 km/sec	11.2 km/sec
Sidereal rotation time	27.322 days	23.9345 hr
Inclination of equator/orbit	6°41’	23°28’
Mean surface temperature	107°C day; -153°C night	22°C
Temperature extremes	-233°C(?) to 123°C (Table 3.3)	-89°C to 58°C
Atmosphere	~10^{4} molecules/cm^3 day 2×10^{5} molecules/cm^{3}night	2.5×10^{19} molecules/cm^3 (STP)
Moment of inertia ($1/MR^2$)	0.395	0.3315
Heat flow (average)	~29 mW/m^2	63 mW/m^2
Seismic energy	2×10^{10} (or 10^{14}?) J/yr†	10^{17}-10^{18}J/yr
Magnetic field	0 (small paleofield)	24-56 A/m

* (Equatorial-ideal)/ideal radii.

† These estimates account for moonquakes only and do not account for seismicity from meteoroid impacts; see discussion of seismic energy in section 3.7.

handle in the reduced lunar atmosphere and gravitational field. Once moving, objects continue moving, although their movements appear to be significantly slower in the lunar environment” (*Aldrin et al.,* 1969).

The Apollo 12 astronauts (*Bean et al.,* 1970) explained that the characteristic “loping” gait seen in all the films of astronauts on the lunar surface was the most natural way to move; heel-to-toe “Earth” walking was more difficult and energy-consuming in the reduced lunar gravity. *Scott* (1973) equated walking on the Moon with the sensation of walking on a trampoline. Although low weight compels this peculiar gait, the mass of an astronaut’s body and personal gear remain unchanged. For this reason it takes considerable exertion to start or stop. “I . . . get under way by thrusting my body forward, as though I were stepping into a wind. To stop, I dig in my heels and lean backward” (*Scott,* 1973).

Energy consumption by the astronauts working on the lunar surface was high (about 1 MJ/hr) but not excessive (*Bean et al.,* 1970). During the Apollo missions no astronauts were placed in the situation of having to negotiate steep slopes; climbing abilities on crater walls or steep hills are still untested. However, the Apollo 12 astronauts reported that recovery from falls was relatively simple in low gravity, despite the awkward suits. “When a fall begins, you first lose your balance rather quickly, particularly if you try to back up, because the ground is uneven and there is a possibility of stepping in holes or on rocks. [Their spacesuits also had an aft displacement of center-of-gravity.] The fall progresses so slowly, though, that there is plenty of time to almost turn around or to catch your footing before you actually fall to the surface. Because a fall begins so slowly on the Moon, it is usually possible to spin around, bend the knees, and recover. Several times, in trying to bend over to get something, we would start to fall over, but the fall progressed so slowly we could start moving our feet and keep moving until they came back under us again” (*Bean et al.,* 1970).

The senses of taste, smell, and hearing are dominated by the artificial environment of the spacesuit and have nothing to do with the Moon.

Touch is secondary, transmitted through the skin of the suit, but is an important factor in an astronaut's ability to move and manipulate. The most critical of the senses is sight, for the lunar environment's most direct impact on a spacesuited astronaut is visual.

Difficulties in visibility were evident in orbit before the astronauts even arrived on the lunar surface. Visibility was poor in areas viewed at low phase angle (i.e., with the sun more or less behind the observer; Fig. 3.1), but topographic details could still be seen. Visibility in subsolar areas is essentially that of zero phase angle. In this condition there is a complete lack of shadows, but albedo differences are clearly visible. Navigation from orbit, using landmarks under these conditions, is very difficult.

From orbit, after a few minutes of adaptation, features on the dark side of the Moon could be viewed clearly in earthshine. Landmark tracking is difficult but not impossible (*NASA,* 1969).

Once on the surface, other visibility problems were noticed. Apollo 11 astronauts Armstrong and Aldrin first commented on this problem: "Distances on the lunar surface are deceiving. A large boulder field located north of the LM [lunar module] did not appear to be too far away when viewed from the LM cockpit. However, on the surface we did not come close to this field, although we traversed about 100 ft toward it. The flag, the television camera, and the experiments, although deployed a reasonable distance away from the LM and deployed according to plan, appeared to be immediately outside the window when viewed from the LM cockpit. Because distance judgement is related to the accuracy of size estimation, it is evident that these skills may require refinement in the lunar environment" (*Aldrin et al.,* 1969).

Right after touchdown, the Apollo 12 astronauts observed that "we were positive of where we were, but it was difficult to pinpoint our exact location because of the limited field of view out the LM windows, because of the general tendency to underestimate distances . . . and because of the difficulty of seeing even large craters beyond a distance of about 100 ft. None of the shadows that were visible in flight, the ones in the bottoms of craters, were visible after touchdown ...it was difficult to find the craters." They also found that "lunar surface visibility was not too unlike Earth visibility, with the exception that the sun was extremely bright . . . shadows were visible only when viewing cross-sun. It was difficult to view down-sun exactly along the zero-phase direction, but this

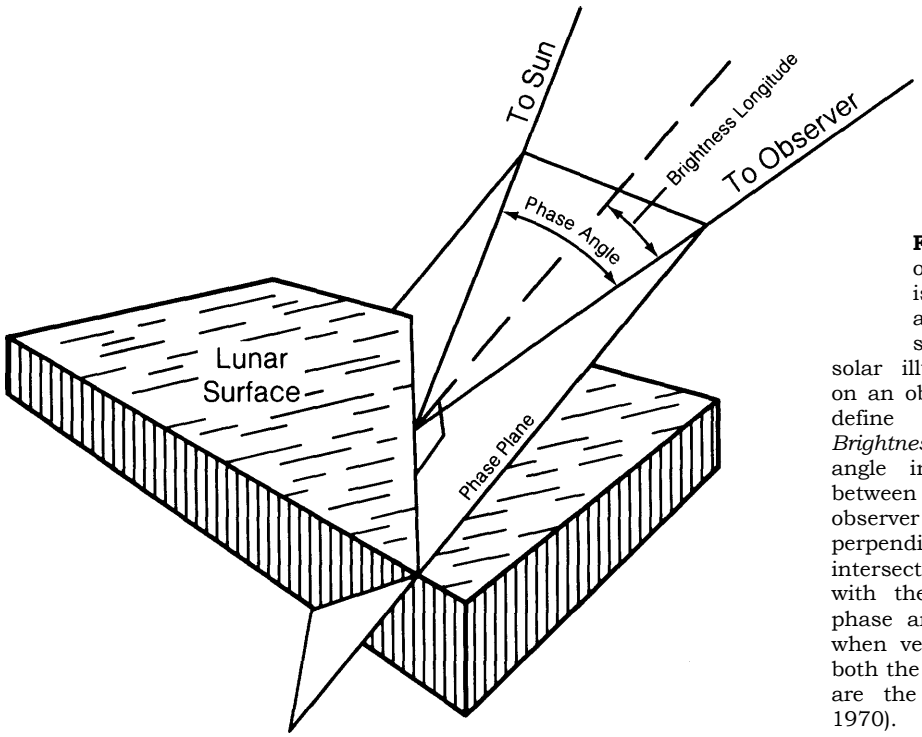

Fig. 3.1. Illustration of *phase angle,* which is the angle between an observer's line of sight and the line of solar illumination impinging on an object. These two lines define the *phase plane. Brightness longitude is* the angle in the phase plane between the light path to the observer and a line perpendicular to the intersection of the ground with the phase plane. Zero phase angle is the condition when vectors to a spot from both the sun and the observer are the same (from *Mutch,* 1970).

deficiency did not hinder normal lunar surface operations because the eyes could be scanned back and forth across these bright zones for visual assimilation. Objects in shadows could be seen with only a slight amount of dark adaptation" (*Bean et al.,* 1970).

"Walking in the up-sun direction posed no problem, although the light was very bright with the sun shining directly into the visor. While walking in the down-sun direction, most objects were visible, but the contrast was washed out. Varying shapes, sizes, and glints were more easily identified in the cross-sun directions" (*Aldrin et al.,* 1969). The Apollo 12 astronauts added the observation that colors were deceptive and changeable, depending largely on sun angle, with the same surface changing from gray to dark or tannish brown during their short 32-hour stay on the Moon (*Bean et al.,* 1970).

In summary, the combination of low gravity, awkward suit mobility, and harsh sunlight without atmospheric filtering leads to significant disorientation in the unfamiliar lunar terrain. Spacesuit improvements and longer periods for acclimatization may improve this situation for future astronauts. A completely different set of visual conditions will be experienced by astronauts who will someday operate on the nighttime lunar surface with illumination by earthshine. The Apollo legacy is only a brief taste of the lunar experience and much remains unknown.

3.3. TERRAIN

"One salient impression we have of our journey was the variety of lunar terranes and geologic structures. We suspect that there is a general lack of appreciation for the complexity of lunar processes and probably of lunar geologic history. We believe that lunar studies will prove fascinating and rewarding for many years and through many programs" (the Apollo 16 astronauts; *Young et al.,* 1972).

The Moon's terrain has been controlled by two factors, high-velocity impacts and volcanism. The mare basins are rimmed with high mountains formed during impact of planetesimals; many of these same basins were smoothed when filled or partly filled with basaltic lavas. Deep channels (rilles) cut the mare surfaces, and faults and wrinkle ridges buckle those same surfaces. All of the Moon's

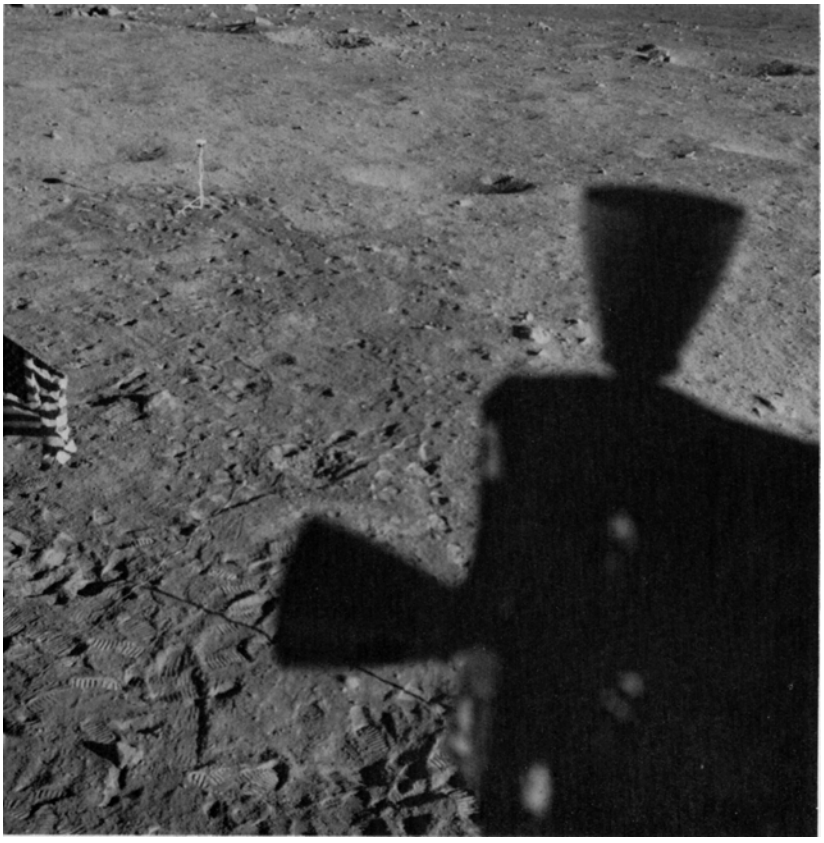

Fig. 3.2. View of the Apollo 11 landing site from a window in the lunar module (NASA Photo AS 11-37-5468). Note the abundance of well-preserved footprints.

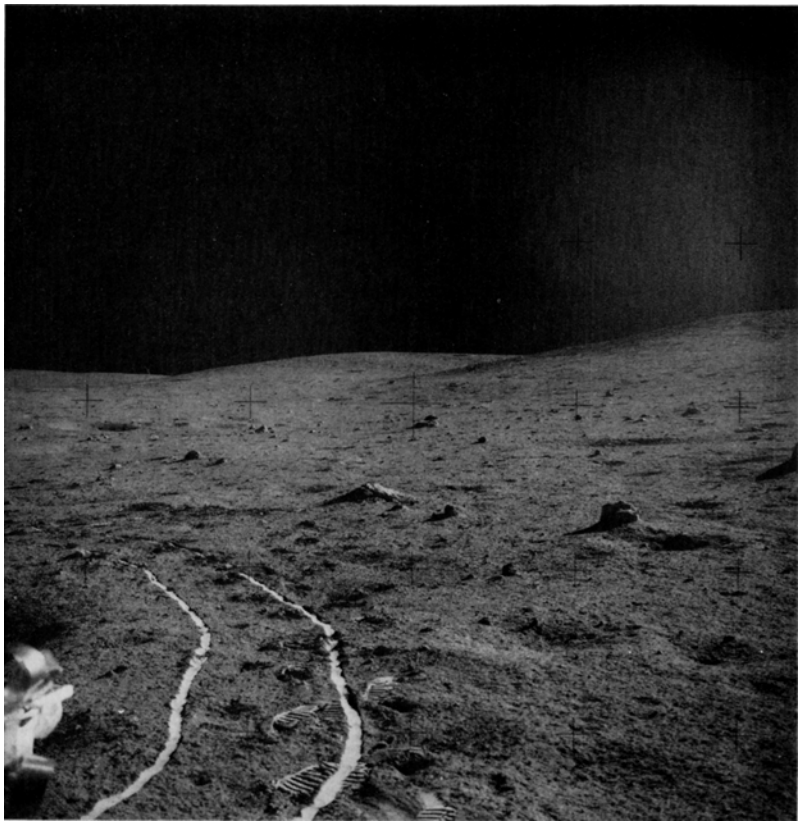

Fig. 3.3. View of a ridge at the Apollo 14 landing site (NASA Photo AS14-64-9058). Slope angles are gentle, but small meter-scale craters are abundant. Sunlight is reflected from the compressed soil in the wheel tracks of the equipment cart (the "modularized equipment transporter"). Note the difficulty of judging distance without familiar visual clues.

surface is cratered, with craters ranging from subdued shallow depressions to sharp-rimmed features littered with large boulders. (For a detailed treatment of crater shapes, sizes, and ages, see Chapter 4.) Nearly all the lunar surface is covered with several meters to tens of meters of loose regolith.

The Apollo astronauts visited a variety of sites on the lunar surface. The examples of terrain described here have been walked upon, driven over, sampled, and tested.

3.3.1. Mare Surfaces

Apollo 11. The Apollo 11 landing site is located on the flat surface of Mare Tranquillitatis. It is, however, far from smooth, being covered with craters ranging in diameter from 0.3 to 20 m (not including the occasional large crater; *Aldrin et al.,* 1969). A fresh, 180-m-diameter, 30-m-deep crater, located 400 m east of the site, is surrounded by a 250-m-wide apron of blocky ejecta with blocks as large as 5 m long. Most of the craters have subdued rims covered with fine-grained regolith (Fig. 3.2). Although there were fresh craters in the area, the astronauts commented that no crater rims were truly sharp. Block fields correspond with crater rays visible on orbital photographs.

Apollo 12. The cratered surface at the Apollo 12 site, on Oceanus Procellarum, was similar to that of Apollo 11. Craters range from very subdued, rimless depressions to sharp, well-defined features. The sharper craters contain concentrations of angular blocks. The small, fresh craters have rubbly rims (*Shoemaker et al.,* 1970). Most of the larger craters near the landing module, ranging from 50 m to 250 m in diameter, have subdued rims; traversing the rim and interior of Surveyor Crater (200 m in diameter, 28 m deep) was easy for the astronauts. Two peculiar mounds were described, each being 1.3 m high and 1.6 m wide, perched on a 6.5-m-diameter base (*Bean et al.,* 1970).

3.3.2. Large-scale Ejecta Ridges

Apollo 14. The Apollo 14 landing site is located on the Fra Mauro Formation, which is characterized by elongate ridges 1 to 4 km wide and a few to tens of meters high. These are large impact-ejecta ridges that radiate away from the Imbrium Basin. Craters

with diameters of 400 m to 1000 m are two to three times more abundant here than in the mare regions. The ridges consist mostly of highland debris, but they contain a variety of mare basalt fragments. One of the ejecta ridges is penetrated by 340-m-diameter Cone Crater, located 1100 m east of the lunar module; its crater rim is littered with blocks 1 to 16 m in diameter with spaces between blocks of several meters. The "smooth" terrain of the site is more or less level over distances of one to several kilometers (Fig. 3.3) but is saturated with craters several tens of meters to hundreds of meters in diameter and meters to tens of meters deep. The walls of older, larger craters have slopes of 10° to 15°.

3.3.3. Lunar Highlands

Apollo 16. The central nearside lunar highlands consist of plains between hilly and "furrowed" mountainous areas (*Muehlberger et al.,* 1972). Adjacent to the heavily cratered plains at the Apollo 16 site are the Descartes highlands; projecting into the area traversed by the astronauts is 540-m-high Stone Mountain. The slopes of Stone Mountain are subtly terraced and have a maximum angle of 18°. Smoky Mountain, located north of the landing site, has a plateau-like top but is steep-sided, with slopes up to 40°.

Both plains and hilly terrain are heavily cratered. Two of the largest and youngest craters studied are 0.5 and 1.0 km in diameter and 100 m and 200 m deep, respectively. Most crater walls are not steeper than 40° to 45°; the walls are covered with loose, thin regolith, boulders, and some outcrops (*Mitchell et al,* 1972b). South Ray Crater, the freshest large crater in the area, has a high block concentration near the crater rim; the astronauts noted that it would have been impossible to drive to the rim because of the blocks (*Young et al.,* 1972). Stone Mountain was also littered with large blocks; here the astronauts had to park their lunar rover in a small crater to keep it from rolling down the slope (Fig. 3.4).

3.3.4. Highlands-Mare Boundaries (Basin Margins)

Apollo 15. This landing site at the eastern margin of the Imbrium Basin was chosen for its

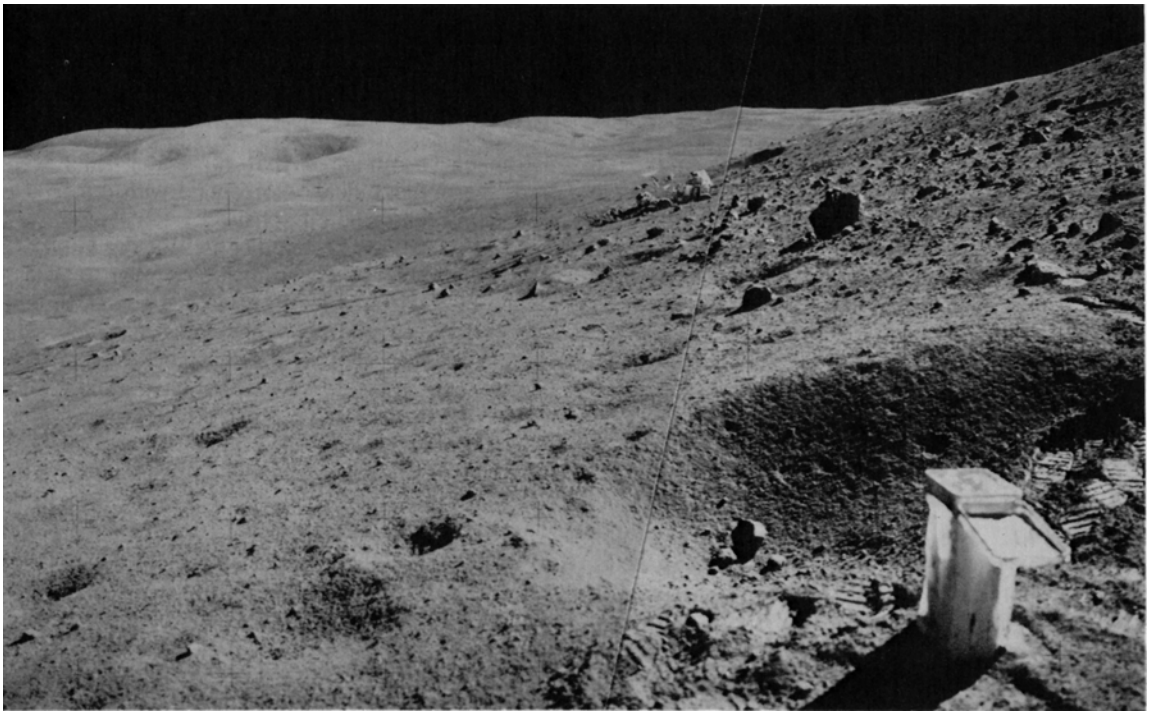

Fig. 3.4. The lunar roving vehicle (LRV), parked below a boulder field on Stone Mountain at the Apollo 16 site (NASA Photos AS16-107-17472 and -17473). The LRV was parked in a small crater to keep it from rolling downhill. Many of the larger boulders are about the size of the tires on the LRV (80-cm diameter). A sample collection container is in the foreground.

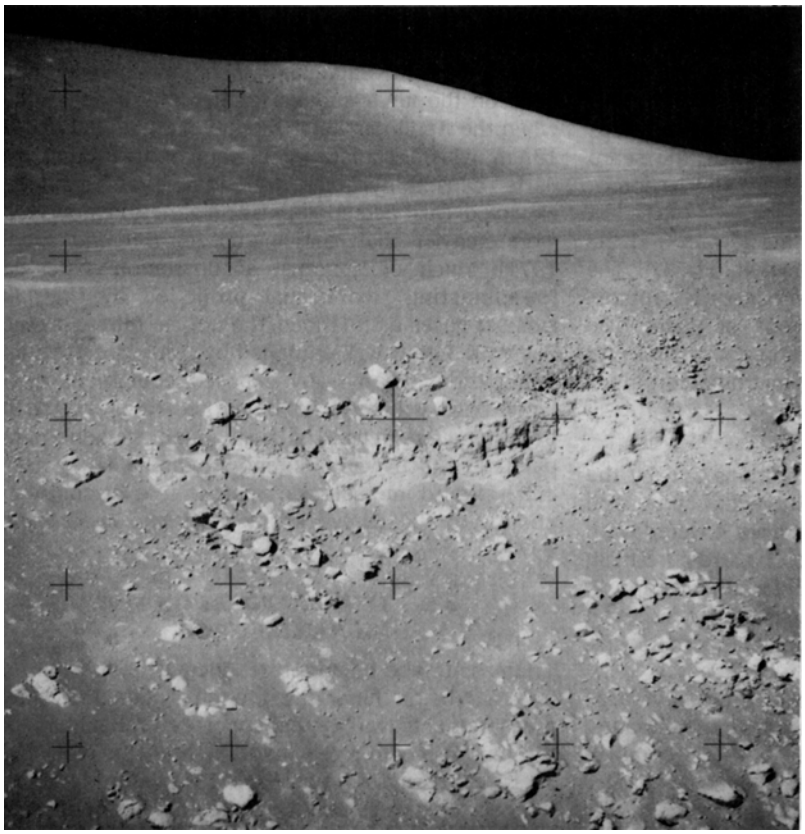

Fig. 3.5. Telephoto view of out-crops of mare lava flows in Hadley Rille at the Apollo 15 landing site (NASA Photo AS15-89-12116). Both massive and thin-bedded lava flows can be seen. The massive flows have well-developed columnar jointing; some of the thin-bedded layers are less than 1 m thick. For scale, the largest boulders in the rille wall are 8 to 10 m in diameter.

geologic and physiographic diversity. The landing was on an embayment of mare lavas that projects into high mountains.

The Apennine Mountains are a chain of rectangular fault blocks that rise 2 to 5 km above the mare surface, rivaling in height many of the mountains of the Earth (*Swann et al.,* 1972). Slopes on these massifs range from >30° on Mount Hadley to 26° on the western flank of Hadley Delta. The steep massifs grade toward the east into low hummocky hills and to the west into a line of hills across a band of mare lava. Numerous "passes" separate these fault blocks and some have been flooded by mare lavas.

The major physiographic feature of this site that would present an obstacle to travel is Hadley Rille. It is 1500 m wide, 400 m deep, and 100 km long. The mare surface slopes gently toward the rille and the regolith is thinner; this is one of the few locations where astronauts came close to sampling bedrock from below the regolith. The rille walls have slope angles of 25° to 30°. There are discontinuous outcrops 35 m to 60 m below the rille rim to the top of talus deposits that partly fill it (Fig. 3.5).

Apollo 17. The last Apollo mission to the Moon visited an area that is physiographically similar to that visited by the Apollo 15 crew: a basin margin where large, steepsided massifs are bounded by narrow valleys flooded with mare basalt flows. Taurus-Littrow Valley is flanked by 2000- and 2300-m-high massifs with average slopes of 25° (*Schmitt and Cernan,* 1973). Many of the craters are buried by regolith emplaced during mass wasting; large (>10 m) boulders have rolled down the slopes of the massifs, leaving visible trails up to 2 km long (*Mitchell et al.,* 1973a). Adjacent to the massifs are low, rounded hills referred to as the "sculptured hills," which are believed to be a separate physiographic province within the highland terrains (*Muehlberger et al.,* 1973). The upper slopes of these hills are 20° to 27°. Below a visible slope change and change in albedo, slopes range from 15° to 20°.

The Apollo 17 area is covered with craters representing a full spectrum of sizes and ages (maturities) (see Chapter 4 for crater descriptions). The valley floor is nearly flat, sloping 1° toward the east. It is, of course, broken by craters, especially by several crater clusters that may be groups of secondary craters (craters formed by lunar fragments ejected from a primary crater, rather than by meteoritic or cometary impacts). It is also partly

covered by a thin avalanche deposit from the South Massif; this deposit consists of fine-grained debris that obscures older craters. The eastern end of the valley is cut by a fault scarp up to 80 m high. This scarp is generally broken into a pair of subdued steps (*Muehlberger et al..,* 1973). Further north, the scarp changes to an irregular wrinkle ridge and is dome-shaped in cross-section.

The contrast between prelanding terrain and the terrain at mission's end is shown in Fig. 3.6. The vehicle tracks and footprints will probably remain visible for hundreds of thousands of years. The equipment left behind will remain for millions of years under the slow battering of micrometeoroids.

3.3.5. Other Parts of the Moon

Parts of the Moon visited by humans and by the unmanned landers, including Surveyor, Luna, and Lunokhod, all have cratered surfaces covered with loose regolith. The most common hazards are fresh craters with steep walls and boulder-strewn rims. In general, the surface can be traversed easily, although diligence will be required to avoid random blocks, fresh craters, and rilles.

We can only infer the nature of the terrain in large craters like Copernicus from Lunar Orbiter images. Traverses may be possible through the complex blocky hills of the central uplift and across crater walls, but little detail will be available until lunar exploration is resumed.

3.4. DUST

"After lunar liftoff . . . a great quantity of dust floated free within the cabin. This dust made breathing without the helmet difficult, and enough particles were present in the cabin atmosphere to affect our vision. The use of a whisk broom prior to ingress would probably not be satisfactory in solving the dust problem, because the dust tends to rub deeper into the garment rather than to brush off" (*Bean et al..,* 1970).

The lunar regolith has grain-size characteristics similar to a silty sand, with mean grain sizes mostly between 45 to 100 μm (Chapter 7). Many of the grains are sharp and glassy; analogies have been made to fine-grained slag or terrestrial volcanic ash. This fine material has very low electrical conductivity and dielectric losses, permitting accumulation of electrostatic charge under ultraviolet (UV) irradiation. The sharp gradient in UV flux across the solar terminator (the boundary between day and night) may generate clouds of electrostatically-supported dust and set them into motion as the terminator moves across the Moon (section 9.2.1 discusses this process in more detail).

Dust accumulation and adhesion to equipment was demonstrated by the examination and recovery of parts from the Surveyor 3 robot lander, which had been on the lunar surface for two and a half years when the Apollo 12 lunar module (LM) landed about 183 m away. Discoloration of painted and aluminum parts, caused by solar irradiation, was found as expected. Dust accumulation and adhesion, however, were heavier than anticipated (*Carroll and Blair,* 1971). Much of the dust accumulation indicated "sandblasting" from dust propelled by the LM exhaust gases as it landed; the optical mirror on the Surveyor 3 craft was damaged by dust accumulation and pitting. Clearly, any exposed equipment at a lunar base will have to be protected or removed from landing areas. Soil was found to adhere to painted surfaces with a strength of about 10^4 dynes/ cm^2, and to metallic surfaces with a strength of about 2 to 3 × 10^3 dynes/cm^2 (*Scott and Zuckerman,* 1971).

3.5. TEMPERATURES ON THE LUNAR SURFACE

Lunar surface temperatures increase about 280 K from just before lunar dawn to lunar noon. Heat flow measurements within the upper several meters of the lunar regolith were made at the Apollo 15 and 17 sites (*Langseth et al..,* 1973), where surface temperatures were also monitored by thermocouples in cables placed several centimeters above the lunar surface. At the Apollo 15 site (26°N, 3.6°E), the maximum temperature was 374 K (101°C) with a minimum of 92 K (-181°C). Temperatures at the Apollo 17 site (20°N, 30.6°E) were about 10° higher (*Langseth and Keihm,* 1977). These observed temperatures are quite close to those determined by Earth-based instruments (maximum = 390 K, minimum = 104 K; *Glasstone,* 1965).

The temperature at lunar noon varies throughout the year because of varying distance from the sun. The noon temperature increases about 6 K from aphelion to perihelion (*Langseth et al..,* 1973).

Langseth and Keihm (1977) describe a large difference in *mean* temperature (i.e., the temperature averaged over a complete day-night cycle) just below the lunar surface. At the Apollo 15 site, the mean temperature at a depth of 35 cm is 45 K higher than that of the surface; at the Apollo 17 site, the difference is 40 K. This increase in the mean temperature is related mostly to the temperature dependence of thermal conductivity of the topmost 1 to 2 cm of lunar soil.

Estimated average surface temperatures and temperature extremes for different areas of the Moon were made by the Lunar Colony Study Group (see *Dalton and Hoffman,* 1972) and are presented in

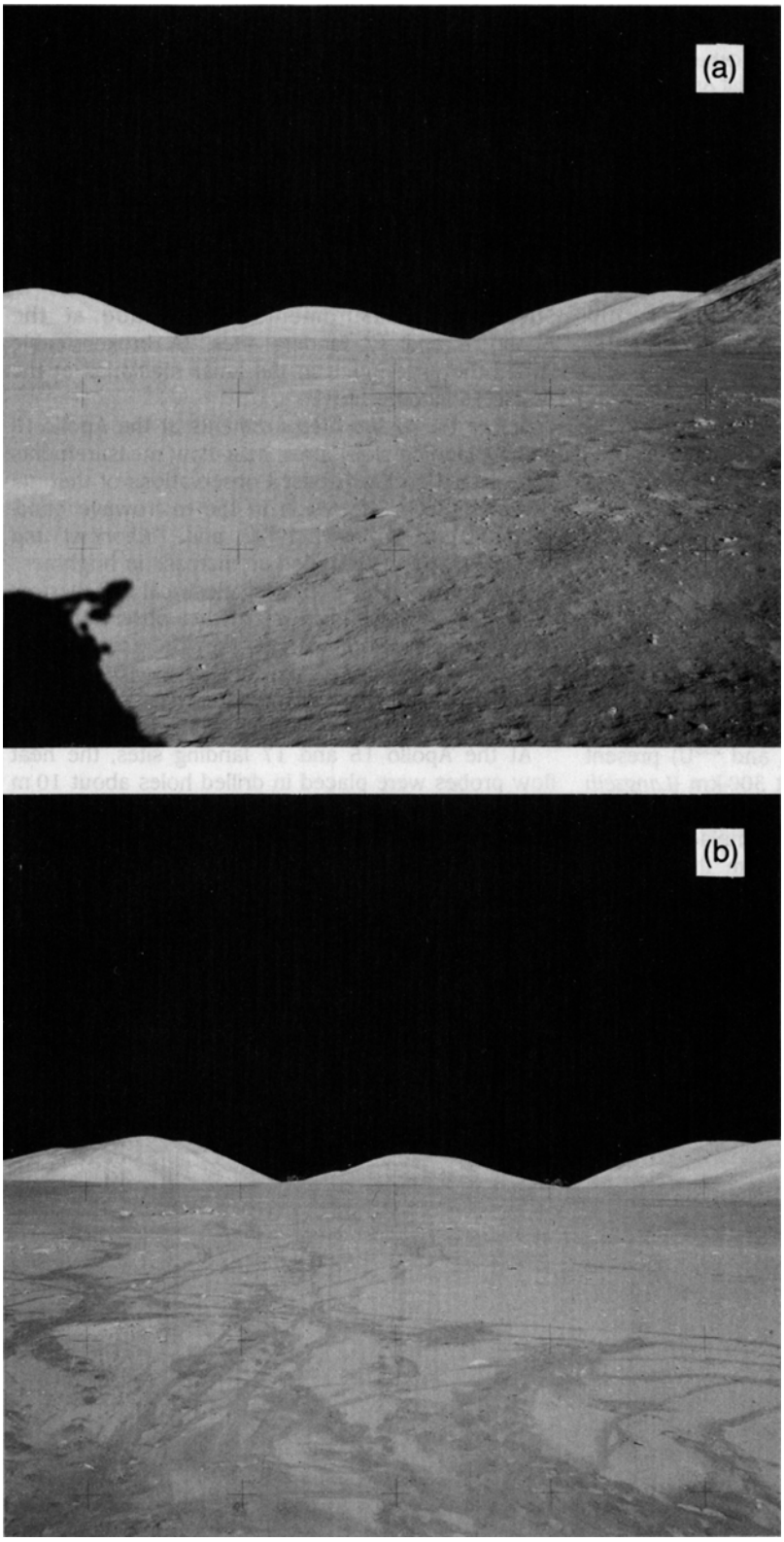

Fig. 3.6. The Apollo 17 landing site **(a)** before (NASA Photo AS17-147-22470) and **(b)** after (NASA Photo AS17-145-22200) the astronaut movements near the lunar module. Note the distribution of tracks and footprints that will remain visible for hundreds of thousands of years. The mountain on the left is 11 km away and 1 km high.

TABLE 3.2. Estimated lunar surface temperatures.

	Shadowed Polar Craters	Other Polar Areas	Front Equatorial	Back Equatorial	Limb Equatorial	Typical Mid-Latitudes
Average temp.	40 K(?)	220 K	254 K	256 K*	255 K	220 < T < 255 K
Monthly range	none	±10 K†	±140 K	±140 K	±140 K	±110 K

* The farside of the Moon is closer to the sun at noon than the nearside is, so it gets ≈1% more solar energy.
† Average temperature has a yearly variation that makes it very cold (T < 200 K) for several weeks.

Table 3.2, along with the estimated very cold temperatures likely to prevail in permanently shadowed polar craters (*J. D. Burke,* 1985). The Lunar Colony Study Group also studied possible temperature variations within craters of lower latitudes and found that the crater floors may be a few degrees warmer than the walls and outer slopes. This has since been verified by thermal infrared mapping (see section 9.2).

3.6. LUNAR HEAT FLOW

The Moon is a small planetary body, and there is good reason to believe that it has lost most of its initial heat during its 4.6-b.y. history. Most of the present heat flux is probably generated by radioisotopes (mainly ^{40}K, ^{232}Th, ^{235}U, and ^{238}U) present in the interior to a depth of about 300 km (*Langseth and Keihm,* 1977). During the Apollo 15, 16, and 17 missions, heat-flow probes were emplaced in the holes left after extracting cores from the regolith. Successful measurements were made at the Apollo 15 and 17 landing sites. (A broken cable ended the experiment in the lunar highlands at the Apollo 16 landing site.)

Before the *in situ* measurements at the Apollo 15 and 17 landing sites, lunar heat-flow measurements were based on Earth-based observations of thermal emissions from the Moon in the microwave band. *Krotikov and Troitsky* (1964) and *Tikhonova and Troitsky* (1969) determined an increase in brightness temperature of 0.6°/cm. Using electrical and thermal properties deduced from microwave observations in the 1-mm to 3-cm range, they interpreted this gradient in terms of a heat flow of 3×10^{-6} W/cm^2 to 4×10^{-6} W/cm^2. This estimated heat flow is very close to that actually measured on the Moon.

At the Apollo 15 and 17 landing sites, the heat flow probes were placed in drilled holes about 10 m apart (Fig. 3.7). Dual probes enabled two independent measurements of heat flow and measurement of the lateral variation of heat flow within the regolith. Each

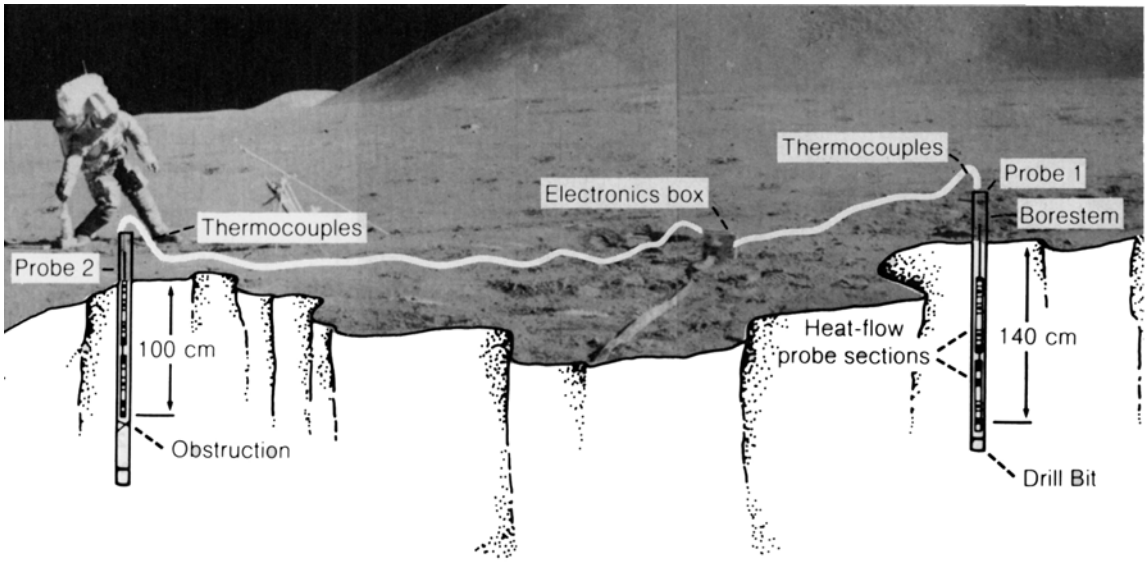

Fig. 3.7. Diagram showing emplacement of lunar heat-flow probes at the Apollo 15 landing site (from *Langseth et al.,* 1972).

probe had two nearly identical 50-cm-long sections; each section had two differential thermometers (accuracy ±0.001 K) that measured temperature differences between points separated by about 47 cm and 28 cm (gradient bridge and ring bridge spacings, respectively; see Fig. 3.8). Measurements of absolute temperature could be made at four points on each probe (*Langseth et al.,* 1972). Additional temperature measurements were made by four thermocouple units in the cables that connected the probes to the central station. Conductivity measurements were made by means of heaters surrounding each of eight gradient-bridge sensors. A heater was energized at 0.002 W and the temperature rise of the underlying gradient sensor recorded as a function of time for a period of 36 hr. The temperature rise and rate of temperature rise was interpreted in terms of the conductivity of the surrounding lunar regolith.

3.6.1. Heat Flow at the Apollo 15 Landing Site

The Apollo 15 heat flow measurements were made in regolith developed on the mare surface 1.8 km east of Hadley Rille and about 4 km north of the base of the Apennine Massif (Hadley Delta). The regolith was sampled to a depth of 237 cm at this location and consists of 42 textural units of mostly fine-grained lunar soil (*Heiken et al..,* 1973). The first probe was inserted to a depth of 1.4 m and the second probe to a depth of 1.0 m; the original planned depth of 3 m could not be reached because of difficult drilling conditions (*Langseth et al..,* 1972).

The subsurface measurements indicated that conductivity must increase substantially with depth, and values of 1.5×10^{-4} W/cm K are found at a depth of 1 m; this increase correlates well with increasing bulk soil density with depth (Chapter 9).

At Hadley Rille, both the rille and the Apennine Front should affect the heat flow, but in opposite ways; both effects are about 5% and thus appear to be self-canceling. The best value for heat flow at this site is an uncorrected value of 3.1×10^{-6} W/cm^2, with an uncertainty of ±20%.

3.6.2. Heat Flow at the Apollo 17 Landing Site

The heat flow experiment at Apollo 17 was located about 200 m west of the landing site and 9 m north of the ASLEP (Apollo Lunar Scientific Experiments Package) on the floor of the Taurus-Littrow Valley. The valley floor consists of irregular, heavily cratered regolith developed on lava flows that partly fill an embayment between 2-km-high massifs; the valley is about 8 km wide at this point. A 400-m-diameter crater is located within 500 m of the heat flow probes. The regolith, sampled to a depth of 292 cm, consists of interbedded fine- to coarse-grained lunar

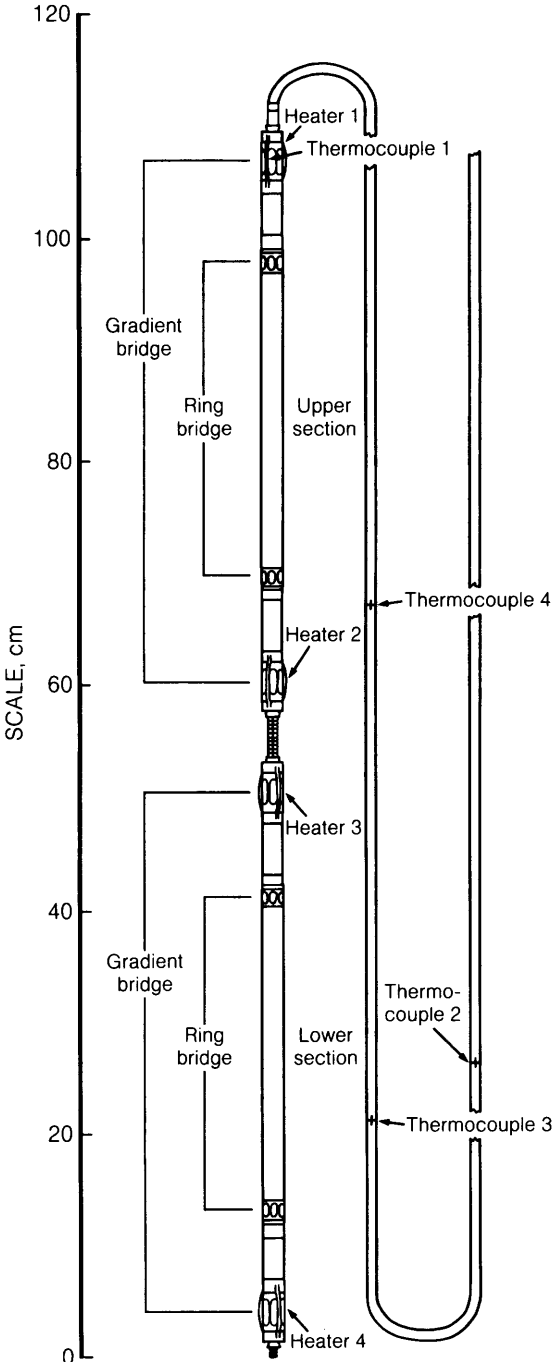

Fig. 3.8. Diagram of a lunar heat-flow probe (after *Langseth et al.,* 1972). Differential thermometers measured temperature differences between gradient bridge and ring bridge spacings in each section. Surface temperature measurements were made by thermocouples in the connecting cable. Activation of the heaters allowed measurement of conductivity.

soil layers. The heat-flow probes were about 11 m apart and emplaced to depths of 2.36 m (probe 1) and 2.3 m (probe 2).

Thermal conductivity measured by the Apollo 17 heat-flow probes ranged from 1.72 to 2.95 × 10^{-4} W/cm K ± 20% (*Langseth et al.,* 1973). This range is related to the bulk density of the regolith. At this site heat flow appeared to be uniform over the probe lengths, with an overall value of 2.8 × 10^{-6} W/cm^2 (probe 1) and 2.5 × 10^{-6} W/cm^2 (probe 2). The large massifs flanking the Taurus-Littrow Valley have a significant effect on the heat flow. It is estimated that a correction of -15% to -20% should be applied; the resulting best heat flow value is 2.2 × 10^{-6} W/cm^2 ± 20%.

3.6.3. Conclusions

The upper 1 to 2 cm of lunar regolith must have extremely low thermal conductivities (1.5 × 10^{-5} W/cm^2), with conductivity increasing 5 to 7 times at a depth of 2 cm. At the Apollo sites, mean temperatures 35 cm below the lunar surface are 40 to 45 K above those at the surface. This is primarily related to the temperature dependence of thermal conductivity in the topmost 1 to 2 cm of lunar regolith (*Langseth and Keihm,* 1977). Thermometers buried 80 cm below the lunar surface show no perceptible variation in temperature related to the lunar day/night temperature cycle. Below these depths, thermal gradients should reflect heat flow from the lunar crust. Figure 3.9 shows the relationship between near-surface day/night temperature fluctuations superimposed on the steady heat-flow profiles in the regolith. It is noteworthy that an insulating blanket of only about 30 cm of regolith is sufficient to dampen out the ~280 K lunar surface temperature fluctuation to ±3 K variation. This indicates that a lunar habitation buried beneath a thick regolith radiation shield will not be subjected to monthly temperature extremes, but rather will have to find an efficient method for dissipating its waste heat.

The heat flow measured at two points on the lunar surface and estimated from microwave emission is 2 to 4 × 10^{-6} W/cm^2, about half that of the average heat flow for the Earth (6.3 × 10^{-6} W/cm^2).

3.7. SEISMIC ACTIVITY

As a result of the Apollo Passive Seismic experiments, the release of seismic energy from the Moon is commonly assumed to be small, only ~2 × 10^{10}

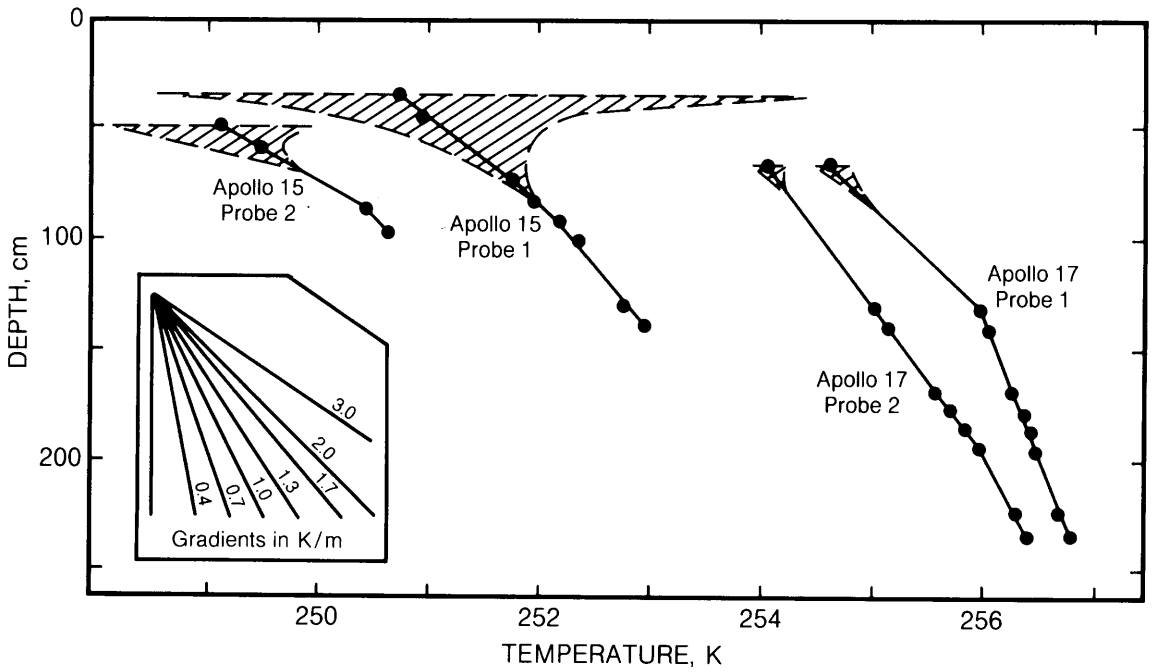

Fig. 3.9. Temperature fluctuations in the lunar regolith as a function of depth (after *Langseth and Keihm,* 1977). Note that the small temperature scale at the bottom of the diagram does not permit plotting of the extreme temperature fluctuations at depths less than ~30 cm; this region is left blank. Hatched areas show day-night temperature fluctuations below ~30 to 70 cm. Below ~50 cm there is essentially no temperature fluctuation due to the lunar day-night temperature cycles, and the steady temperature gradients recorded are due to internal lunar heat flow.

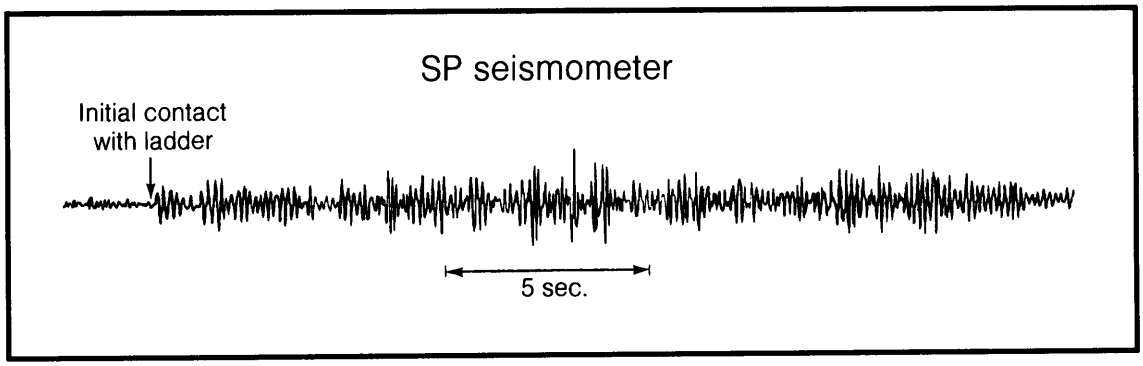

Fig. 3.10. The short-term (SP) seismometer could detect all of the Apollo 11 astronaut movements on the lunar surface. This figure shows the signal recorded by the SP seismometer, ~17 m away, as Neil Armstrong climbed the ladder of the lunar module (after *Latham et al.,* 1970c).

J/yr compared to Earth's 10^{17} to 10^{18} J/yr (e.g., *Goins et al.,* 1980). This is the lower value listed in Table 3.1. Note, however, that larger but rarer moonquakes may not have occurred during the eight years of lunar seismic monitoring, and the actual average lunar seismic energy could be as high as 10^{14} J/yr (*Nakamura,* 1980); this is the queried higher value in Table 3.1. In either case, the Moon's low seismic activity, coupled with extremely low elastic wave propagation losses (e.g., low attenuation, sometimes referred to as "high Q"), means the Moon is an extremely quiet place, even though seismic events and the resulting elastic "sounds" carry for long distances through the rock and soil with great clarity. (Note that there is no sound transmission through the air as the atmosphere is too thin.) The Apollo 11 passive seismic instrument clearly recorded Astronaut Armstrong climbing the ladder into the LM (Fig. 3.10). This sensitivity to seismic energy because of low attenuation gave rise to the phrase "the Moon rings like a bell," as seen in the characteristically long seismic signatures of moonquakes and of meteoroid impacts on the Moon (Fig. 3.11).

Over the eight years of Apollo passive seismic recording, the largest recorded moonquakes have Earth-equivalent magnitudes of about 4. The sources of seismicity on the Moon include the monthly *deep-focus moonquakes* caused by Earth-Moon tidal stresses (sometimes appearing as moonquake swarms), a few stronger (but rarer) *shallow moonquakes* (also known as high-frequency teleseisms or "HFT") that may be due to tectonic processes, and *meteorite impacts* (*Hood et al.,* 1985; *Dorman et al.,* 1978; *Goins et al.,* 1978; *Latham et al.,* 1978; *Nakamura,* 1978). *Nakamura et al.* (*1982*) also distinguish some small *thermal moonquakes* that may be due to thermal degradation of young lunar surface features (e.g., thermal cracking of fresh boulders around young craters). Although there were only about four or five shallow moonquakes per year during the period of lunar seismic monitoring, they account for most of the seismic energy released in the Moon (*Nakamura,* 1980). Table 3.3 lists the events recorded during the nearly eight years of seismic station operation during the Apollo program.

Seismic events due to meteoroid impact vary widely in energy. Meteoroid impacts of all energies tend to be most common when meteoroid showers peak (*Dorman et al.,* 1978), particularly among the largest meteoroid impacts that tend to occur in the months of April through July. The largest recorded impacts, in July 1972 and May 1975, represented meteoroids of about *5* t. In all, seven meteoroid impacts of 1 t or more were observed within five years during lunar seismic monitoring (*Latham et al., 1978; Dorman et al.,* 1978). Major impacts are very rare (Chapter 4), but the effects can be widespread; for example, a major landslide visited at the Apollo *17* site in the northern hemisphere was probably caused by impact of debris from the crater Tycho (~100 m.y. old), which is some 2000 km away in the southern hemisphere (*Arvidson et al.,* 1976). Landslides or slumping of crater walls may be triggered seismically as well as by impact. Even though such events are rare it may be prudent to locate permanent lunar establishments away from potentially unstable slopes (section 9.1).

3.8. POLAR ENVIRONMENT

The Apollo missions and most of the Lunar Orbiter missions concentrated on the equatorial regions of the Moon, leaving the poles little better known than in the pre-Apollo era. Image resolution by Lunar Orbiter 4 was only ~100 m at the poles; also, many

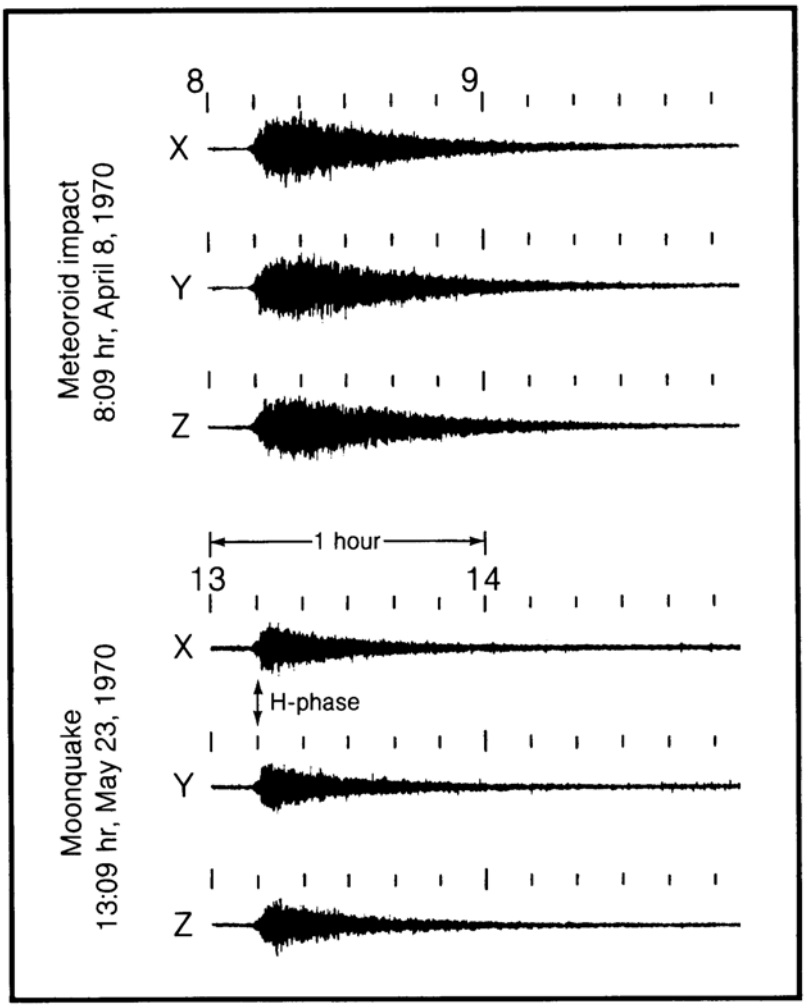

Fig. 3.11. Natural seismic activity on the Moon. Top: probable meteoroid impact of April 8, 1970; bottom: moonquake of May 23, 1970, with probable focal depth of 800 km. Such deep moonquakes have monthly cycles and are apparently due to tidal forces. One difference between the moonquake and the meteoroid impact is the presence of a distinct "H-phase," recorded as a primarily horizontal (X,Y) motion, suggesting a shear-wave mechanism (after *Latham et al.,* 1972). The Z motion is vertical.

features in the polar areas were obscured by shadows. Much of the speculation about environmental conditions at the poles has been summarized by *J. D. Burke* (1985).

The very small inclination of the Moon's equator to the ecliptic (1°32'; see Fig. A3.2) leads to the most interesting of these speculations, that there may be ice preserved in permanently shadowed craters or valleys where surface and subsurface temperatures may be relatively constant and as low as 40 K. Debate over the presence or absence of lunar polar ice has developed over several years; summaries of the problems involved (reradiated sunlight, solar wind sputtering, and whether ice can be protected by regolith blankets) are given by *Arnold* (*1987*) and by *Svitek and Murray* (1988). Similarly, there may be elevated "mountains of perpetual light" at the poles, which could serve as sites for continuous solar power collection. However, the combination of rough terrain plus the slight but not insignificant inclination of the Moon's spin axis makes such features unlikely. If nothing else, our ignorance of the lunar poles should spur future exploration.

3.9. ATMOSPHERE

The lunar atmosphere is extremely tenuous. The undisturbed gas concentration is only about 2×10^5 molecules/cm^3 during the lunar night, falling to perhaps 10^4 molecules/cm^3 during the lunar day (*Hodges et al.,* 1975). This is about 14 orders of magnitude less than Earth's atmosphere, a difference so extreme that the Moon is often said to have no atmosphere at all—a misstatement that arises from the terrestrial perspective. Much of our present understanding of the lunar atmosphere is based on

TABLE 3.3. Summary of the Apollo passive seismic experiment data (after *Latham et al., 1978*).

Period of Observation		
1 station (July-Aug., Nov. 1969 - Feb. 1971)		1.27 yr
2 stations (Feb. 1971 - July 1971)		0.48 yr
3 stations (July 1971 - Apr. 1972)		0.73 yr
4 stations (Apr. 1972 - Sept. 1977)		5.44 yr
Total		7.92 yr
Number of Seismic Events Detected		
	Total*	Major Events†
Artificial impacts	9	5
Meteoroid impacts	1700‡	95
Shallow moonquakes (HFT)	32‡	7
Deep moonquakes		
confirmed	973‡	9
unconfirmed	1800‡	2
Unclassified events	7300‡	0
Total	11,800‡	118

* The total does not include signals detected only by the short-period seismometers of each station, or the large number of signals detected by the Apollo 16 station only.
† "Major events" are those signals with amplitude >10 mm at two or more stations.
‡ These numbers represent estimated data as compiled by *Latham et al.* (1978). Final numbers of 1743 meteoroid impacts, *28* shallow moonquakes, 3145 deep moonquakes, and 7633 unclassified events are given by *Nakamura et al.* (1982).

theory, not because the instruments deployed during the Apollo missions were inadequate (they were in fact extremely accurate and sensitive) but rather because the gases released during the missions flooded the data. This problem is easy to visualize when it is considered that the total ambient lunar atmosphere is only about 10^4 kg, and each Apollo landing released as much gas while on the Moon (*Vondrak,* 1974). The six Apollo landings delivered six times as much gas to the lunar surface as there is in the ambient atmosphere.

3.9.1. Contamination

The results of the Cold Cathode Gage experiments in Apollo missions 12, 14, and 15 clearly show the ease with which the ephemeral lunar atmosphere is contaminated (*Johnson et al.,* 1970, 1972). These gages were extremely sensitive, and were easily driven off-scale by the waste gas clouds emitted from the astronauts whenever they approached within a few meters of the experiment. Contamination remained evident long after the astronauts left.

Figure 3.12 shows the fluctuation of gas concentration at the Apollo 14 landing site for 10 lunar days (about three-quarters of a year) following the landing. Discontinuities in the curves shown are due to periods when the instrument was turned off for fear of high-voltage arcing, and days 6 through 8 are not shown because they would clutter the diagram between days 5 and 9. At the first lunar day after the astronauts left (day 2), there was a sharp rise in gas concentration as the area around the landing site was heated up. This suggests that a large amount (perhaps 10%) of the lunar module exhaust gas (a mixture of about 20% H_2O with a wide variety of C-H-O-N species; *Freeman et al.,* 1972) was adsorbed onto the lunar surface during the first lunar night after the astronauts departed, to be released rapidly as the sun rose again. These adsorbed gases were probably widely scattered, because the adsorptive capacity of lunar soil is low (10^{-4} to 10^{-5} g gas/g soil) and lunar rocks are 10 to 100 times less adsorptive than soil (*Vondrak,* 1974). Release profiles for the subsequent lunar days probably reflect losses from both the lunar module and the contaminated equipment and regolith. These later losses appear to be very long-lived, with a time constant of about three or four months.

A miniature mass spectrometer, the Lunar Atmospheric Composition Experiment (LACE), was placed in the Taurus-Littrow Valley during the last Apollo landing (Apollo 17). This instrument was able to show that helium, neon, and argon are native to the lunar atmosphere. Hydrogen is also native, but the hydrogen data were swamped by contamination (*Hoffman et al.,* 1973). Contamination makes interpretation of the data difficult, but much effort has been put into this interpretation and we now have a reasonably good understanding of what the lunar atmosphere contains.

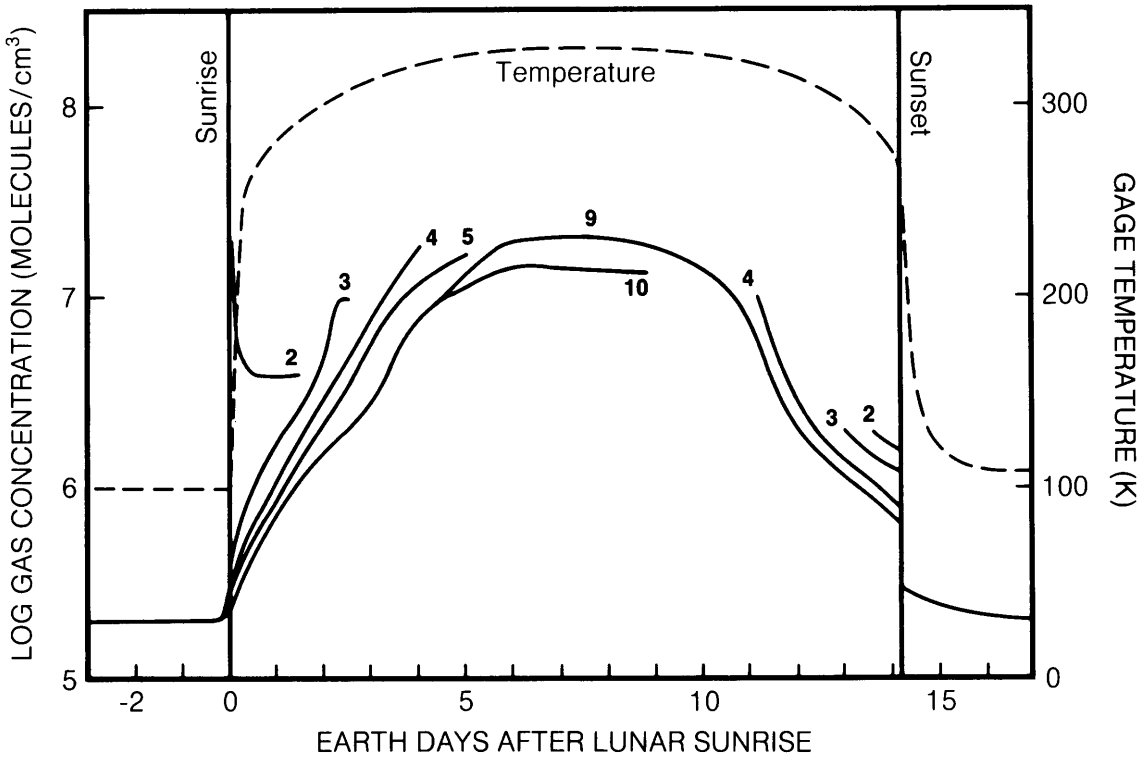

Fig. 3.12. Variation in total gas concentration (molecules/cm^3) in the near-surface atmosphere at the Apollo 14 landing site, over nine lunar days (curves numbered 2 to 10) following the Apollo 14 landing (counting day 1 as the day of the landing, when no data were obtained). Surges in gas concentration during the lunar daytime are not a feature of the undisturbed lunar environment (see Fig. 3.13); these daytime gas surges are due to the solar heating of soil and equipment at the landing site with resulting contaminant gas release. To avoid crowding, days 6 to 8 are not shown; these curves fall between those for days 5 and 9. Data were not collected through a full day cycle until day 9, for fear of high voltage arcing at midday temperatures. The monthly temperature cycle is also plotted (after *Johnson et al.,* 1972).

3.9.2. The Real Lunar Atmosphere

The major constituents of the ambient lunar atmosphere are neon, hydrogen, helium, and argon. Neon and hydrogen are derived from the solar wind. Helium is mostly derived from the solar wind, but ~10% may be radiogenic and lunar in origin (*Hodges,* 1975). Argon is mostly ^{40}Ar that is derived from the radioactive decay of lunar ^{40}K (only about 10% of the argon is ^{36}Ar of solar wind origin). Table 3.4 lists the most probable abundances of these and a few other species in the undisturbed lunar atmosphere.

The numbers listed in Table 3.4 are subject to several causes of both variability and unreliability. First, the contamination problem is particularly severe for the daytime gas determinations. Second, the variability in abundance of the impinging solar wind will affect the solar-wind species. Gases escape thermally (H_2, He) or they are ionized and lost (Ne, Ar) within about four months (10^7 sec; *Johnson et al.,* 1972; *Hodges et al.,* 1974); these processes allow recycling of the lunar solar-wind atmosphere within weeks to months. Third, the lunar day-night temperature differential becomes smaller at higher latitudes, resulting in smaller differences between daytime and nighttime atmospheres as the poles are approached. The fluctuations correlative with latitude are summarized for the four most abundant atmosphere species (^{20}Ne, He, H_2, and ^{40}Ar) in Fig. 3.13. The Apollo 17 LACE data for He and ^{40}Ar used for this figure are particularly well constrained; the data for ^{20}Ne and H_2 are less precise.

Both Table 3.4 and Fig. 3.13 show a major distinction in the behavior of argon compared to the lighter simple gases. Argon abundances in the atmosphere drop rather than rise during the lunar night, and do so rather gradually. This is because argon is a condensable gas at lunar nighttime temperatures, whereas neon, helium, and hydrogen are not. The complex C-H-O-N gases are also

condensable and follow argon in behavior. Note that the noncondensable gases (Ne, He, H_2) increase in concentration by night, and decrease by day; this is because the noncondensable gas concentrations vary as an inverse power of surface temperature ($T^{-5/2}$; *Hodges et al.,* 1974), resulting in their concentration on the night side. As found in the Cold Cathode Gage experiments of Apollo 12, 14, and 15, the lunar module contaminant gases are almost completely condensable (Fig. 3.12).

3.9.3. The Past and Future of the Lunar Atmosphere

On Earth, Precambrian rocks (especially those rocks older than about 1200 m.y.) provide evidence of major changes in the chemical composition of earlier terrestrial atmospheres. In contrast, there is little in the lunar geologic record to provide detailed evidence for any variation in the Moon's past atmosphere. There has been some speculation,

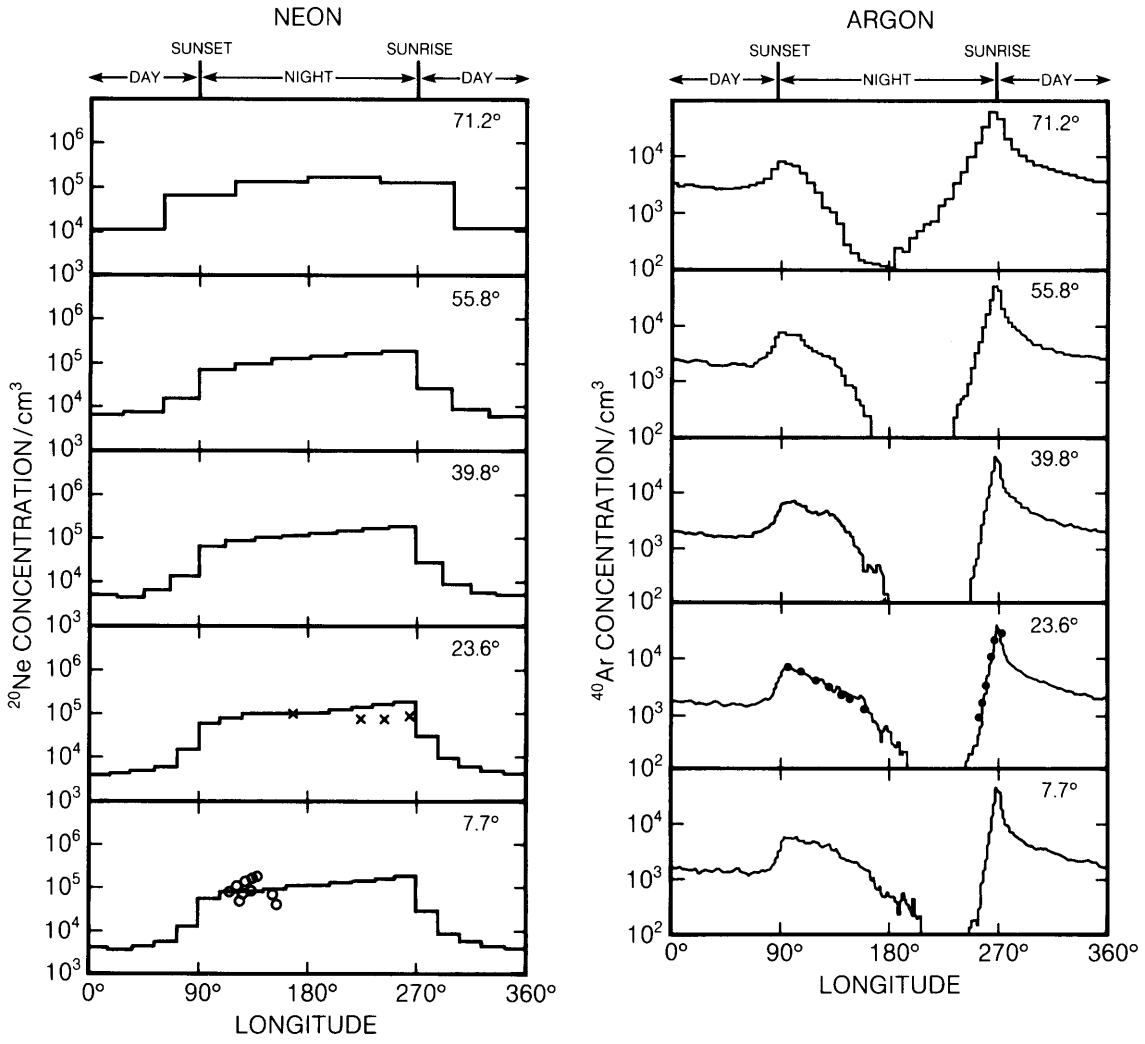

Fig. 3.13. Calculated variations in abundances of the four principal lunar atmospheric gases over day/night cycles at five latitudes (circumferential bands at 7.7°, 23.6°, 39.8°, 55.8°, and 71.2° away from the equator). The day/night cycle is depicted with sunrise at 270° long., the subsolar point at 0° (or 360°), and sunset at 90°. The calculated ^{20}Ne gas concentrations at 7.7° and 23.6° lat. are compared with actual data from Apollo 16 and Apollo 17, respectively; the calculated ^{40}Ar concentration at 23.6° is compared with the Apollo 17 data. Line thicknesses for He and H_2 allow for ±5°C uncertainty in the nighttime temperature (after *Hodges et al.,* 1974).

however, that the lunar atmosphere may have been about 5×10^7 times as massive as it presently is at some time in the past 10^8 years. This speculation is based mostly on an apparent lack of some micrometeoroid effects in buried soils, leading to a model that calls for a thicker atmosphere to screen out impactors in the 10^{-7} to 10^{-11} g range (*Chernyak, 1978; Hughes,* 1978).

Much more certain are the possible effects of large-scale human operations on the lunar surface. Irreversible pollution of the lunar atmosphere is a real possibility. Each Apollo mission left behind a mass of gases equivalent to the ambient lunar atmosphere; many of these gases have large molecular weights and are condensable. Some of the Apollo gases may prove to be particularly pernicious, and permanent pollution may already have occurred.

Vondrak (1974) points out that most gases are presently removed from the lunar atmosphere through ionization from interaction with the solar wind and the interplanetary electric field. Thermal escape (heating to escape velocity) is a much less significant process. However, if the lunar atmosphere were >100 times as massive as it presently is, the roles of these two processes would be reversed. At a total mass of about 10^7 to 10^8 kg these loss mechanisms would reach steady or declining rates and the Moon would obtain a long-lived atmosphere (Fig. 3.14). The Apollo missions did not cause such a drastic change, and even a small lunar base would

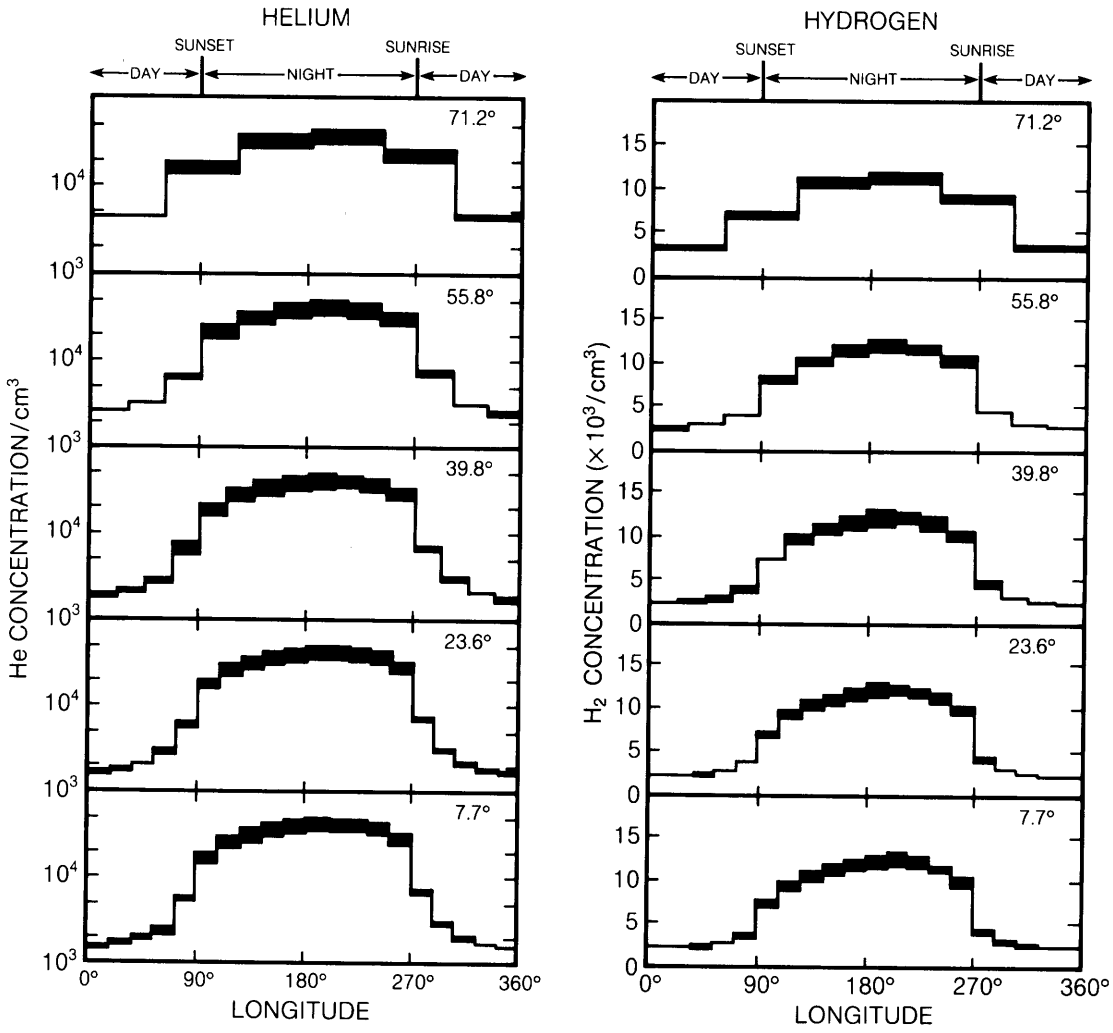

Fig. 3.13. (*continued*)

TABLE 3.4. Gas abundances and some scale heights in the lunar atmosphere.

	Abundances (molecules/cm^3)		Scale Heights*	
	Daytime	Nighttime	Daytime	Nighttime
^{20}Ne	$\sim 4 \times 10^3$ to 10^4	10^5	100 km	25 km
He	$\sim 8 \times 10^2$–4.7×10^3	4 to 7×10^4	511 km	128 km
H_2	~ 2.5–9.9×10^3	10^4 to 1.5×10^5	1022 km	256 km
^{40}Ar	$\sim 2 \times 10^3$	to $<10^2$	55 km	
CH_4	$\sim 1.2 \times 10^3$			
CO_2	$\sim 10^3$			
NH_3	$\sim 4 \times 10^2$			
$OH+H_2O$	~ 0.5			

*"Scale height" refers to the altitude at which the amount of an atmospheric constituent drops to 1/e (0.368) of its surface abundance in an isothermal atmosphere.

Based on calculations reported in *Hodges et al.* (1974), *Hodges* (1973), *Hoffman and Hodges* (1975), *Mukherjee* (1975), and *Johnson et al.* (1972).

fall short of such a consequence; however, extensive lunar operations may be capable of releasing sufficient waste gases to create such an atmosphere. *Vondrak* (1974) suggests that any process producing more than 100 kg/sec of gas will produce a long-lived lunar atmosphere. He concludes his analysis with a summary of Kraft Ehricke's suggestion that buried 1 kt nuclear detonations might be used to create caverns of about 40 m diameter on the Moon, each cavern yielding about 10^7 kg of oxygen. The problems of polluting the present lunar atmosphere would certainly be swamped by such a massive planetary manipulation. Any possible benefits of such a project would have to be carefully weighed against the loss of a very unique high-vacuum environment, a loss that would produce a major degradation in many lunar-based science and engineering activities.

3.10. METEOROID BOMBARDMENT

The term "meteoroid" is used for a naturally occurring solid body, traveling through space, that is too small to be called an asteroid or a comet. Meteoroids with diameters less than about 1 mm (and hence with masses less than about 10^{-2} g) are commonly classified as micrometeoroids. The suffix

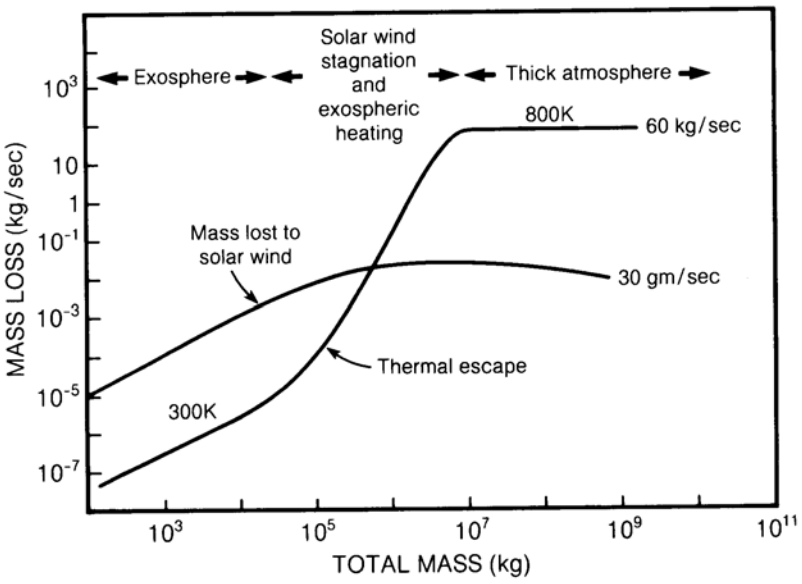

Fig. 3.14. Variations between thermal and electrostatic gas loss mechanisms as a function of lunar atmosphere mass (hypothetical; after *Vondrak,* 1974). A pure oxygen atmosphere (mass 16 amu) is assumed for this model; thermal escape gas losses from the thick atmosphere are probably overestimated because the model atmosphere is assumed to be isothermal. Relative gas temperatures for thermal escape at $\sim 2 \times 10^3$ kg and at $\sim 10^8$ kg are shown.

"ite" (e.g., meteorite) is used for meteoroids that have fallen through an atmosphere and been recovered. However, the terms "meteorite" and "meteoroid" are often used generically as in, for example, the "meteorite complex."

From the size and frequency distributions of meteoroids discussed in Chapter 4, it can be estimated that micrometeoroids of about milligram mass should be expected to strike lunar features as large as facilities and equipment almost yearly; impacts by smaller objects will be more frequent, and by larger objects more rare. Although much is known about the size-frequency distributions of meteoroids, the consequences of these objects for prolonged space missions are still poorly understood.

3.10.1. Meteoroid Velocities and Impact Rates

Direct measurements of meteoroid impact were obtained in the vicinity of the Moon by Lunar Orbiters 1 through 5 (Table 2.1). These orbiters were ringed by sets of pressurized semicylinders made of 0.025 mm metal with pressure-sensitive switches to record perforation by meteoroids. Data from the five orbiters, corrected for geometry and exposure orientation, suggest 0.16 perforations per m^2 per day (*Gurtler and Grew,* 1968). This is about half the perforation rate in comparable experiments flown on Explorer spacecraft in near-Earth orbit. *Erickson* (1969) suggests that this difference is related to an increase in meteoroid flux caused by the Earth's gravitational attraction. In addition, the increase in velocity resulting from the Earth's pull causes the near-Earth impacts to be more penetrating.

Meteoroid velocities have been measured near Earth by photographic and radar tracking. If corrected to constant meteoroid mass, the velocities of meteoroids at the Moon can be calculated to range from 13 to 18 km/sec (*Zook,* 1975). The meteoroid flux at the lunar surface shows a significant enhancement from small meteoroids (<1 μm) traveling toward the Moon from the sun and a somewhat lesser enhancement of large particles (>1 μm) arriving from the direction in which the Earth is traveling (*Fechtig et al.,* 1974; *Zook and Berg* 1975; *Oberst and Nakamura,* 1986). Whichever side of the Moon is facing into the direction of the Earth's motion in its orbit around the sun will be more exposed to the larger and more hazardous meteoroids (*Gurtler and Grew,* 1968).

3.10.2. Meteoroid Distributions in Lunar Orbit and on the Lunar Surface

The size distributions and frequencies of micrometeoroids are discussed in section 4.1.3 and shown in Fig. 4.14. The distribution shown in Fig. 4.14 is fairly well defined as far as the spacecraft-collected data are concerned. Although there has been some suggestion that the meteoroid flux may be much higher on the lunar surface than it is in lunar orbit, such a variation has not been established (*Fechtig et al.,* 1974). There are also indications that the present meteoroid flux, as measured by spacecraft, may be more than an order of magnitude higher than the time-averaged prehistoric flux calculated from impact microcraters on lunar samples (*Hartung and Storzer,* 1974; *Cour-Palais,* 1974; *Grün et al.,* 1985). More data are needed to constrain the current and past meteoroid fluxes on the Moon.

3.10.3. Meteoroid Hazards

Meteoroids of about 10^{-6} g can produce craters of 500 μm diameter in metal. In most materials, depth of the crater will be comparable to or less than the diameter; however, fracturing effects in brittle materials may extend the damage to greater depth. Figure 3.15 shows the number of perforations per day that may be expected for a given thickness of Be-Cu metal as used in the spacecraft meteoroid detectors (*Gurtler and Grew,* 1968). Two to three millimeters of a tough composite material is relatively effective shielding against damage by micrometeoroids in the milligram mass range.

Although rarer, the impacts of larger meteoroids are a more significant hazard. For meteoroid masses of about 1 g, craters of centimeter scale and somewhat lesser depth are formed; the damage

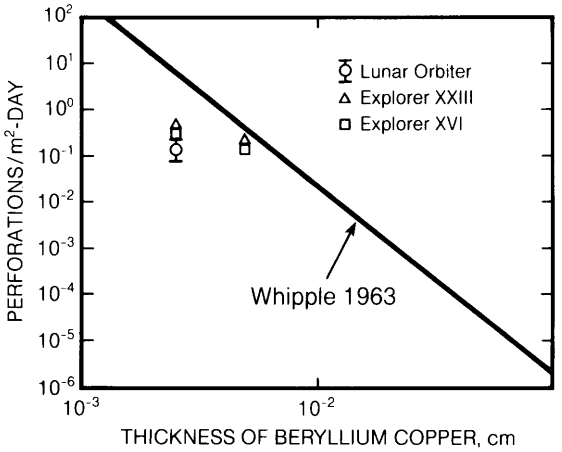

Fig. 3.15. Hazards of perforation by meteoroids in lunar orbit as a function of metal thickness (after *Gurtler and Grew,* 1968). Explorer and Lunar Orbiter data are compared with *Whipple's* (1963) predicted curve, modified to compare with the beryllium copper used on the spacecraft instruments.

inflicted may be more than cosmetic. The probability of such a meteoroid striking an astronaut on the lunar surface is very small—about one chance in 10^6 to 10^8 for one year of cumulative time exposed on the surface. The most significant hazard, therefore, is to large and critical structures—habitats, base support facilities, processing plants, or research instruments—that are expected to last on the lunar surface for many years.

The actual risk to an object exposed on the Moon is difficult to estimate. Risk is commonly expressed as some compound measure of both probability and consequences (*Lowrance,* 1976). The current probabilities of impact by meteoroids of particular sizes are now fairly well known, but the consequences of damage will depend very much on the nature and function of each component for which risk must be assessed. For a large but inert structure, the consequences may be very small; for a small but vital life-support package, the consequences may be great. Meteoroid hazards at a lunar base therefore cannot be fully constrained until a detailed base layout is considered.

3.11. IONIZING RADIATION

The space around the Moon contains many types of ionizing radiation: large fluxes of low-energy solar-wind particles, smaller fluxes of high-energy galactic cosmic rays, and rare but occasionally intense particle fluxes emitted by solar flares. The radiation fluxes and energies typically span at least eight orders of magnitude. Radiation energy is traditionally expressed in units of electron volts (eV) or multiples of eV (such as keV, MeV, or GeV) with 1 eV = 1.6022×10^{-12} erg. The lunar radiation environment also changes with time, usually reflecting the level of solar activity, such as the modulation of galactic cosmic rays and the irregular emission of energetic particles from the sun.

Three major types of radiation at the Moon are discussed here: the solar wind, solar-flare-associated particles (also called solar energetic particles or solar cosmic rays), and galactic cosmic rays. The radiation consists mainly of protons and electrons with some heavier nuclei. These particles interact with the Moon in different ways, depending on their energy and composition, resulting in penetration depths that vary from micrometers to meters. The results of interactions with exposed lunar rocks and soils also vary considerably; the effects include solar-wind implantation, heavy-nuclei tracks, spallation reactions, and the generation of secondary neutrons and gamma rays. A summary of the three radiation types in terms of their energies, fluxes, compositions, and lunar interaction depths is given in Table 3.5. The numbers in this table are averages or more probable ranges, and most of the values can vary widely with time and/or energy.

Not discussed below are other types of gamma, electron, antimatter, and other charged-particle radiation that have been observed in space around the Earth-Moon system. These particles are present in such low fluxes or low energies that their interactions with the Moon are very difficult to detect, and some have not been well characterized. The gamma rays that come from galactic sources or that are emitted from the sun in large solar flares have low fluxes. There also are several varieties of low-energy particles (usually <0.1 MeV for electrons and <1 MeV for protons) that have been seen near the Earth-Moon system or that have been inferred from studies of lunar samples. Some particles near the Moon have origins other than the sun or the "galaxy." These include electrons emitted by Jupiter's magnetosphere or nuclei like ^{40}Ar that have diffused from the lunar surface and then been ionized and carried along with plasmas near the Moon. During the rare times that the Moon is in the Earth's magnetotail, even some terrestrial particles can reach the lunar surface.

The majority of the observations about radiation presented here were collected by instruments on spacecraft beyond the Earth's magnetosphere; these observations are representative of what hits the Moon. The Earth's strong magnetic field and thick atmosphere make it hard to use Earth-based methods to study these radiations, even though observations on Earth led to their discovery. For example, the galactic cosmic radiation was identified by ionization chambers carried aloft with Victor Hess on balloons in 1911-1912, and Forbush's ionization chambers detected high-energy (GeV) particles from the sun in the 1940s (*Pomerantz and Duggal,* 1974).

The Earth's magnetic field scatters particles back into space, except near the magnetic poles where even low-energy solar particles reach the Earth's atmosphere. The ionization at the top of the Earth's atmosphere by large fluxes of particles absorbs cosmic radio noise ("polar cap absorption" or PCA). Since 1952, riometers have been used routinely to measure polar cap absorptions caused by solar particles (see, e.g., *Pomerantz and Duggal,* 1974). The Earth's atmosphere is thick enough (1000 g/cm^2) that very few cosmic-ray particles penetrate to the surface. Among those that reach the surface are the weakly-interacting muons and a few neutrons. Ionization chambers and neutron detectors on the Earth's surface have monitored galactic and solar cosmic radiations since 1936, with energy discrimination being provided by the strength of the geomagnetic field at various locations. While used

TABLE 3.5. Summary of the three major types of radiation in the lunar environment.

Type	Solar Wind	Solar Cosmic Rays	Galactic Cosmic Rays
Nuclei energies	~0.3–3 keV/u*	~1 to >100 MeV/u	~0.1 to >10 GeV/u
Electron energies	~1–100 eV	<0.1 to 1 MeV	~0.1 to >10 GeV/u
Fluxes (protons/cm^{2}sec)	~3×10^8	~0–10^6†	2–4
Particle ratios‡			
electron/proton	~1	~1	~0.02
proton/alpha	~22	~60	~7
L ($3 \le Z \le 5$)/alpha	n.d.	<0.0001	~0.015
M ($6 \le Z \le 9$)/alpha	~0.03	~0.03	~0.06
LH ($10 \le Z \le 14$)/alpha	~0.005	~0.009	~0.014
MH ($15 \le Z \le 19$)/alpha	~0.0005	~0.0006	~0.002
VH ($20 \le Z \le 29$)/alpha	~0.0012	~0.0014	~0.004
VVH ($30 \le Z$)/alpha	n.d.	n.d.	~3×10^{-6}
Lunar Penetration Depths			
protons and alphas	<micrometers	centimeters	meters
heavier nuclei	<micrometers	millimeters	centimeters

* eV/u = electron volts per nucleon.
† Short-term SCR fluxes above 10 MeV; maximum is for the peak of the August 4, 1972 event. Flux above 10 MeV as averaged over ~1 m.y. is ~100 protons/cm^{2}sec.
‡ Ratios often vary considerably with time for the solar wind and SCR particles and with energy for SCR and GCR. The symbols L (light), M (medium), H (heavy), VH (very heavy), etc., are historical terms for nuclei charge (Z) groups greater than 2 in the cosmic rays.
n.d. = not determined (usually because the ratio is too low to measure). Composition data from *Feldman et al.* (1977) and *Bame et al.* (1983) for the solar wind, *McGuire et al.* (1986) for the SCR, and *Simpson* (1983) for the GCR.

mainly to study the galactio cosmic rays, about once a year these surface detectors observe signals called "ground level enhancement" (GLE) due to solar particles. Such effects as PCA and GLE are not present on the Moon with its very weak magnetic fields and tenuous atmosphere, but are mentioned here because of the considerable information that they have given us about cosmic-ray particles.

3.11.1. Solar Wind

Besides the radiant energy continuously emitted from the sun, there is also a steady plasma emission. This plasma consists of an equal number of ions and electrons with an embedded magnetic field that expands from the solar corona (*Hundhausen,* 1972). The solar wind streams outward from the sun through the solar system creating interplanetary magnetic field lines that have spiral shapes because of the sun's rotation. The solar wind is electrically neutral, and the composition of the nuclei in it is approximately that of the sun. At a distance of 1 A.U. from the sun, the mean energy of the, solar-wind ions is ~1 keV/u (keV/atomic-mass-unit or, for nuclei, keV/nucleon), and all particles move at nearly the same velocity. The solar-wind velocity typically ranges from 300 to 700 km/sec, and its particle concentrations normally range from 1 to *20* per cm^3 (*Feldman et al.,* 1977). The solar-wind proton flux generally ranges from 1×10^8 to 8×10^8 protons/ cm^2 sec.

The composition of the solar wind is not well known, especially for heavier nuclei. The short-term alpha-particle-to-proton ratio has been observed to range from ~0 to 0.25, although the longer-term average over periods of months is in a smaller range, 0.037-0.055 (*Hundhausen,* 1972; *Bame et al.,* 1983). Both direct satellite measurements and analyses of artificial materials exposed at the lunar surface (*Walker,* 1975) have helped to characterize abundances of heavier nuclei in the solar wind. The abundance ratios given in Table 3.5 are from *Feldman et al.* (1977) and *Bame et al.* (1983). As noted in section 3.9 and in Chapter 8, the solar wind is the main source for several volatile elements in the lunar atmosphere and on the lunar surface, such as H, He, C, and N, that are otherwise rare on the Moon. The solar wind also serves as a minor cause of long-term erosion of lunar samples by producing sputtering reactions on exposed surfaces (the main agent of lunar erosion is the cratering produced by micrometeoroid impacts).

3.11.2. Solar-Flare-Associated Particles

The sun also produces intermittent high fluxes of energetic charged particles that are associated with some major solar flares. These solar-flare-associated particles are also called solar energetic particles or solar cosmic rays (SCR). As only the higher-energy particles are emphasized here and some other writers use the expression "energetic particles" for lower-energy species, the term solar cosmic rays or SCR will be used below.

Solar-cosmic-ray particles can be accelerated either in the sun's corona or in interplanetary space. These particles reach the Earth-Moon system in less than a day. After a big solar flare, electrons with energies of ~0.5-1 MeV arrive at 1 A.U., usually traveling along interplanetary field lines, within tens of minutes to tens of hours. Solar protons with energies of 20-80 MeV usually arrive within a few to ~10 hours (*Van Hollebeke et al.,* 1975). Some high-energy SCR particles can arrive in as little as 20 minutes from flares on the sun's western hemisphere that are well connected to the Earth (see, e.g., *Rust,* 1982). For many flares, mainly low-energy (~10-100 keV) electrons reach the Earth (*Simnett,* 1974). Very large flares also can accelerate electrons and energetic nuclei to relativistic velocities (i.e., traveling close to the speed of light).

The locations of most flares producing these high-energy particles that reach the Earth are in the sun's western hemisphere (*Pomerantz and Duggal,* 1974), although in some cases the flare is not visible from the Earth, making prediction of the solar particle event more difficult. The nature of solar flares and how they accelerate particles to high energies are not very well known, although recent observations are giving us a better picture of high-energy processes in solar flares (see, e.g., *Rust,* 1982; *Chupp,* 1988). In several cases, particles are accelerated to high energies in interplanetary space by multiple reflections between two converging shock fronts (*Pomerantz and Duggal,* 1974). We shall not discuss solar flares further or the origin or propagation of these solar high-energy particles but will concentrate on SCR properties as observed near the Earth, at 1 A.U. from the sun.

Because relativistic electrons (E > 0.5 MeV, the rest mass of an electron) and nuclei with energies above a few MeV/u are emitted only in large fluxes by major flares at the sun (*Pomerantz and Duggal,* 1974), they are present at the Moon only a small fraction of the time. Very few SCR particles are present during periods of minimum solar activity; most are emitted during the time near solar maximum. Figure 3.16 shows the occurrence of major fluxes of SCR particles for three 11-year solar cycles along with a smoothed curve for the sunspot number (the sum of the number of individual sunspots, plus 10 times the number of sunspot groups). Sunspot curves have been used as one indicator of solar activity (see *Pomerantz and Duggal,* 1974). Solar-cosmic-ray particles are seldom emitted during the period of the 11-year solar cycle when solar activity is near a minimum but can be present near the Moon at any time when the sun is fairly active, usually when the sunspot number is above ~50. However, the sunspot number is only a qualitative indicator of SCR fluxes (*Goswami et al.,* 1988).

The temporal distribution of solar protons during a month when the sun was very active is shown in Fig. 3.17. This period is more active than most but shows some typical features for the fluxes of solar protons at 1 A.U. Detectable fluxes of high-energy protons are only present for a few days after a solar flare. The flux of low-energy solar protons persists for longer periods of time. The flux of SCR particles rises fairly rapidly right after a flare and then decays at rates that vary with their energy, with higher-energy particles decaying faster. The periods of maximum SCR fluxes are typically a few hours. During a solar particle event, the directions and amounts of anisotropy of the SCR particles can vary (*Pomerantz and Duggal,* 1974). The largest anisotropy usually occurs in the early phases of an event, with the maximum flux generally about 50° west of the sun-Earth line, the direction of the solar wind magnetic field at 1 A.U. The lower-energy particles near the end of a SCR event tend to arrive more isotropically.

The particle compositions in typical SCR events are given in Table 3.5. Most nuclei are protons or alpha particles. Electrons usually arrive ahead of these nuclei because they travel faster at these energies (*Simnett,* 1974). There are some heavier nuclei, of which the more easily ionized elements are enriched relative to those with high ionization potentials (*McGuire et al.,* 1986). The ratios of various elements in the SCR can vary within an SCR event and from event to event (*McGuire et aL,* 1986). Elemental ratios can also vary with energy (*McGuire et al.,* 1986; *Reedy et al.,* 1983). Very unusual elemental ratios (e.g., high $^3He/^4He$) have been observed in some small events, but these events account for a very small fraction of the total fluence at the Moon over long periods of time.

As indicated in Fig. 3.17 and shown in Fig. 3.18, the SCR particle energy spectrum drops rapidly with increasing energy, most particles having energies below ~30 MeV. The spectral shape varies during an SCR event and, as shown in Fig. 3.18, can be very different from event to event. Most SCR events have soft spectra with few high-energy particles. However,

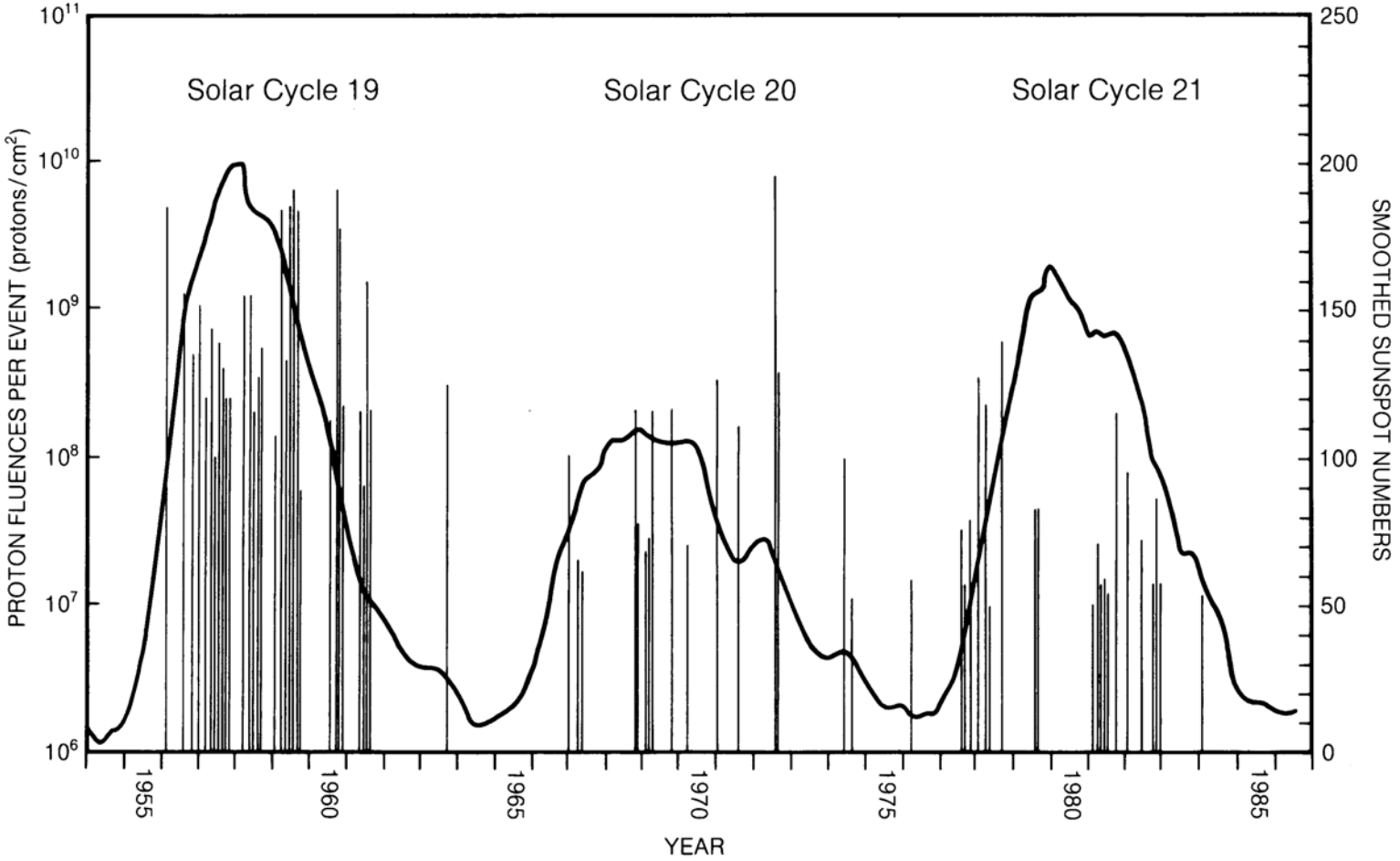

Fig. 3.16. Vertical lines mark individual event-integrated fluxes of solar protons above 30 MeV (*Reedy,* 1977; *Goswami et al.,* 1988). The curve shows the smoothed sunspot number, an indicator of the level of solar activity, over three 11-year solar cycles.

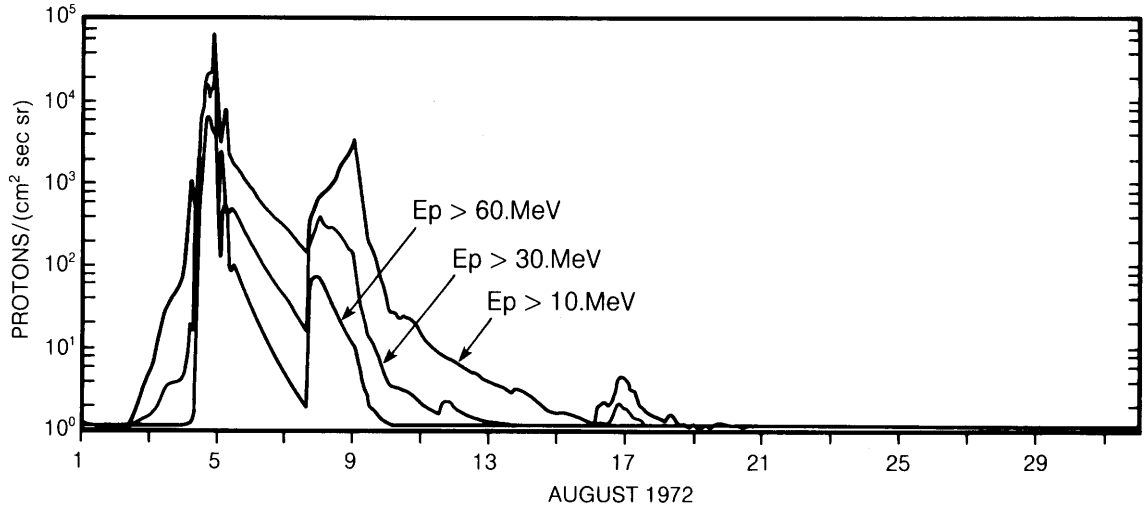

Fig. 3.17. Time distributions of the fluxes of solar protons (protons per cm²-sec-steradian) integrated above energies of 10, 30, and 60 MeV during August 1972, a month when the sun was very active (*Kohl et al.,* 1973). Note the sharp (few hours) rise and the long (days) decay in the proton fluxes during each event.

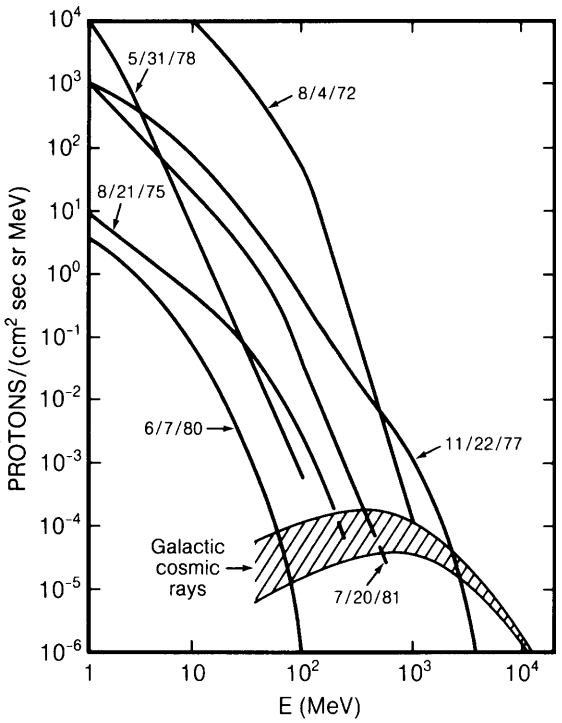

Fig. 3.18. Solar-cosmic-ray (SCR) proton fluxes vs. energy. The highest proton fluxes observed at a given energy during each event are shown as a function of energy for six representative medium to large solar-particle events. Also shown are the usual ranges of GCR proton fluxes over a typical 11-year solar cycle (see also Fig. 3.19). For the August 4, 1972 event, the time-of-maximum fluxes below 100 MeV are based on the integral fluxes in Fig. 3.17 and the fluxes above 100 MeV are from *Simnett* (1976). The maximum fluxes shown for the five other events are from *McGuire and von Rosenvinge* (1984), except that the fluxes above 400 MeV for the November 22, 1977 event are from *Debrunner et al.* (1984). Note the large differences in proton fluxes and spectral shapes among different events.

a few events can have large fluxes of high-energy particles that extend to GeV or higher energies (see, e.g., *Pomerantz and Duggal,* 1974). It is these rare events, with high fluxes of very energetic particles, that are of the most serious concern for men and material exposed in space or on the lunar surface. The intensity of high-energy particles in these rare, intense SCR events is such that neutron monitors or ionization chambers on the surface of the Earth record very large increases (up to 90 times normal levels during the February 23, 1956 event) for several hours during the peak of the event (*Pomerantz and Duggal,* 1974). On the Moon, an astronaut caught outside his shielded habitat during such an event could easily receive a debilitating or lethal radiation dose in a few days; at peak fluxes the dose may cause nausea and vomiting within an hour (*Rust,* 1982). Prediction of SCR events and ready access (on ~30 minutes notice) to a buried shelter will be requirements for safe long-term astronaut exposure on the lunar surface.

Our ability to accurately estimate the probabilities of very large SCR particle fluxes is limited by the fact that observation of such particles has only been done qualitatively since 1942 and by direct measurements using detectors on satellites since the 1960s (*Pomerantz and Duggal,* 1974; *Reedy,* 1977; *Goswami et al.,* 1988). Rough intensity estimates of the solar protons emitted during solar cycle 19 (1954-1964) were made by *Reedy* (1977) using indirect measures of the relative intensities of solar-proton events and using the solar-proton-produced radioactivities in lunar rocks. Some of the indirect estimates of solar-proton intensities during this period were low by factors of 3 to 5, and this solar cycle appears to have had a much larger flux of solar protons and many more events with very high fluxes than the two more recent solar cycles (*Goswami et al,* 1988). During the last two decades there has only been one very large solar-particle event, in August 1972. It should also be noted that solar-particle events occurred in 1942 (two events), 1946, and 1949 that, based on terrestrial GLE data, were larger than any seen from 1957 to 1988 (*Pomerantz and Duggal,* 1974).

Thus our ability to predict the probabilities of large solar-particle events is limited by the fact that such events are rare and have seldom been measured (cf. *Goswami et al.,* 1988; *King,* 1974). The data for the last few solar cycles suggest that large particle events with integral proton fluences above 10^{10} protons/cm^2 are fairly rare. Estimates for the probabilities of solar-particle events with proton fluences above 10^{10} protons/cm^2 vary widely (*King* 1974; *Lingenfelter and Hudson,* 1980; *Goswami et al.,* 1988). The activities of long-lived radionuclides made in lunar rocks by SCR particles have been used to determine the average fluxes of solar protons over time periods of 10^4 to 10^7 years (*Reedy,* 1980). These average solar-proton fluxes and the absence of detectable solar-proton-produced ^{14}C in tree rings over the last 7000 years has led *Lingenfelter and Hudson* (1980) to conclude that extremely large solar proton fluxes are rare and that the probability curve as a function of integral event fluence takes a sharp drop for fluences above ~10^{10} protons/cm^2.

However, several of the intense events observed since 1953, such as the February 23, 1956 event with a very hard spectrum and the August 4, 1972 event, would have been hazardous to humans exposed in space (*Rust,* 1982; *Letaw et al.,* 1987). The existing data indicate that there could be several hazardous solar-particle events per solar cycle, and that there is only a period of a few years around solar minimum when such events are unlikely. Habitats shielded under 2 m (about 400 g/cm^2) of densely packed regolith are a minimum requirement for a lunar base; for full protection from the rare gigantic flare events, shielding of about 3.5 m thickness will be necessary (*Silberberg et al.,* 1985).

3.11.3. Galactic Cosmic Rays

The main matter in the solar system that originates far from the solar system is that in the galactic cosmic rays (GCR). The GCR particles with energies below ~10^{15} eV come from our galaxy, and their flux at the Earth is very isotropic (*Simpson,* 1983). Energies of GCR particles extend up to ~ 10^{20} eV, although such ultrahigh energies are very rare. The actual sources of GCR particles and the reasons for their great energies are not well known (*Simpson,* 1983). The GCR nuclei typically take ~ 10^7 years to reach us and, during that time, have passed through ~5 g/cm^2 of interstellar matter. Spallation reactions during their interstellar passages result in a significant abundance of the rare elements lithium, beryllium, and boron and enhancements in other minor elements, such as those just below iron (see composition in Table 3.5). The amount of antimatter in the GCR is low, with the measured ratio of antiprotons to protons in the range of 10^{-3} to 10^{-4} (*Simpson,* 1983).

The main source of variations in the fluxes and energies of GCR particles at the Moon is solar activity. Magnetic fields carried by the solar wind as it expands from the sun cause the GCR particles to lose energy as they penetrate into the solar system. During a typical 11-year solar cycle, the flux of GCR particles with energies above 1 GeV/u varies by a factor of 2, with the highest GCR fluxes during periods of minimum solar activity. As shown in Fig. 3.19, the modulation of the GCR energy spectrum is greatest at low energies, and GCR particles with energies above ~10 GeV/u are barely affected by the magnetic fields in the solar wind.

The actual amount of modulation of GCR particles varies from solar cycle to solar cycle, and the curves in Fig. 3.19 are based on measured GCR fluxes during the last two solar cycles (*Reedy,* 1987). Deviations from this range of GCR fluxes are expected only during very rare periods of unusually low or high solar activity (*Reedy et al,* 1983). The largest possible flux of GCR particles at the Moon would be for a long period of very low solar activity, at which time the GCR particle flux would approach that of the local interstellar medium. Estimates for the interstellar GCR particle flux vary, and the interstellar GCR flux curves in Fig. 3.19 span the range of estimates (*Reedy,* 1987). Galactic-cosmic-ray particle fluxes as a function of energy at the lunar surface probably will never exceed the local interstellar space curve. The last time that the GCR particle flux was much above the typical range was probably during the

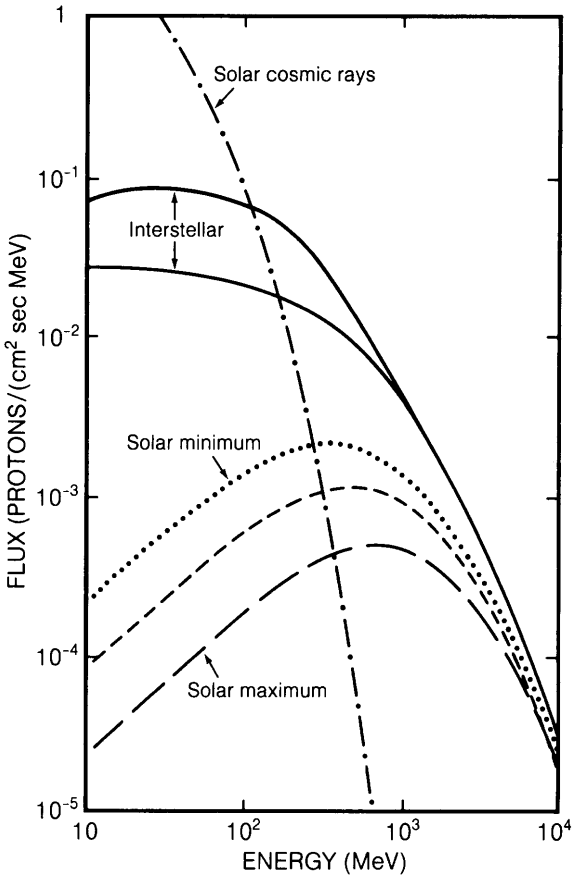

Fig. 3.19. Galactic-cosmic-ray proton fluxes vs. energy (from *Reedy,* 1987). The curves for minimum and maximum of solar activity are the same as those in Fig. 3.18 but are integrated over 4 π solid angle. The dashed curve between "solar min." and "solar max." is the GCR flux near the Moon averaged over an 11-year solar cycle. The two solid curves at the top represent the range of estimates for GCR particle fluxes in interstellar space, which would be the GCR flux near the Moon if there were no solar activity. The dot-dashed curve shows for comparison the long-term (thousands to millions of years) averaged fluxes of solar protons.

Maunder Minimum, which was a period of very low solar activity lasting from the years 1645 to 1715 (*Reedy et al.,* 1983).

3.11.4. Modes of Interactions with the Moon

All energetic particles interact with matter by a few well-known processes. Most energetic particles and all neutrons can induce nuclear reactions with the nuclei in the lunar surface. These nuclear reactions range with the energy of the incident particle from neutron capture and elastic scattering to high-energy spallation. The products of these nuclear reactions range from the initial target nucleus to nuclei far from the target and also can include a wide range of secondary particles, such as neutrons, pions, gamma rays, and various nuclear fragments.

The energy of the incident particle determines what nuclear reactions are possible and the probabilities for these reactions. Nuclear reactions, especially elastic-scattering reactions, are the only way that energetic neutrons can interact (although particles can escape from the Moon and thus stop interacting with it). Typical energetic (MeV) particles will induce nuclear reactions with an interaction mean free path of ~100 g/cm^2. Thus even the highest-energy GCR particle will have interacted before passing through ~1000 g/cm^2 of matter, which is the thickness of the Earth's atmosphere or of ~5 m of lunar regolith.

The nuclear reaction induced by a high-energy particle (E > ~10 MeV) usually initiates a cascade of particles. Typically, a number of secondary particles, and possibly even the incident particle with degraded energy, are emitted by the initial nuclear reaction. Most low-energy secondary charged particles are stopped by ionization-energy losses before reacting, but the secondary neutrons and higher-energy charged particles can induce additional nuclear reactions (*Armstrong and Alsmiller,* 1971; *Reedy and Arnold,* 1972). The secondary particles, especially neutrons, made in the cascades started by GCR particles, are an important part of the lunar radiation environment.

One way that charged particles interact with matter is to ionize atoms and molecules, thereby losing energy. Most low-energy (below ~30 MeV/u) charged particles are slowed down so fast (within <1 g/cm^2) that they usually are stopped before they can induce a nuclear reaction. The heavy nuclei in the GCR, especially those with higher charges, also are rapidly stopped by ionization energy losses. It is because of their short ranges (the distances over which they are stopped) that the penetration depths of heavy nuclei, as shown in Table 3.5, are much less than those of protons and alpha particles. The nuclei that are stopped are then implanted in that material, and most SCR and all solar-wind nuclei end up as implanted species in the upper layers of the Moon. Most GCR protons induce reactions, as the range of a 400 MeV proton is about equal to its interaction mean free path (~100 g/cm^2), and most GCR protons have energies much higher than 400 MeV and very long ranges in the Moon.

The energetic particles in the lunar environment also induce a variety of radiation damage effects. The

radiation damage induced by nuclei with Z > 20, near the end of their range, is so high that it can be seen by transmission electron microscopy in certain minerals. Simple chemicals can preferentially dissolve the damaged areas in these minerals (*Walker,* 1975*; Reedy et al.,* 1983)*;* the etched holes are called *tracks.* Tracks from the iron group (VH) nuclei typically have lengths of 10-20 μm. Electrons can occasionally become trapped in metastable energy states and are very slowly released. The light emitted when these trapped electrons are released during heating is called *thermoluminescence* (*Walker,* 1975), and the amount of light released can sometimes be used to estimate how long a sample was exposed to radiation.

Energetic particles can displace the nuclei in the target material. If the displaced atom is on the surface, it can be removed from that material, a process called *sputtering.* On the lunar surface, erosion of exposed surfaces is mainly by micrometeoroid impacts and not by sputtering (*Walker,* 1975). If the dose of energetic particles to which a material is exposed is high enough, the structure of the material can be changed. The very outer layers (about 0.05 μm thick) of some lunar grains are amorphous because of their bombardment by the intense flux of solar-wind nuclei (*Walker,* 1975).

While similar processes occur on the Earth, two major differences between the Earth and the Moon affect the nature of these interactions. The Earth has a very strong magnetic field that deflects almost all SCR particles and most GCR particles. The only places on Earth where the magnetic fields are not important are above the geomagnetic poles. Magnetic fields on the Moon are generally so weak that even the very low-energy ions in the solar wind can hit the lunar surface. The other major difference is the Earth's atmosphere, which has a thickness of about 1000 g/cm^2. The atmosphere is thick enough that the dose of particles at the surface is much lower than that at the top of the atmosphere. The cascade of particles in the atmosphere is partially affected by its low density, as pions can travel far enough before interacting that they decay into muons, while on the lunar surface with its density of *~2* g/cm^3 the pions usually react with nuclei, producing secondary neutrons, before decaying (*Lingenfelter et al.,* 1961, 1972). Therefore the number of secondary neutrons in the lunar surface is higher than that in the atmosphere above the Earth's magnetic poles by a factor of *~50%,* and the flux of muons on the Moon is much less than that for the Earth.

Solar wind. Solar wind particles have such low energies (~1 keV/u) that they only interact with the lunar surface by rapidly stopping (in much less than a micrometer) in the uppermost layer. This interaction also can produce sputtering and, if the dose of solar wind particles is intense enough, can change crystalline regions on the surfaces of grains into amorphous layers (*Walker,* 1975). *A*s noted by *Walker* (1975), the amount of solar wind atoms hitting the Moon over 4 b.y. is about equal to the number of lunar atoms in the top 10 m of the lunar regolith. However, many solar wind atoms are not retained and eventually escape into space (see section 3.9.2). The solar wind is the major source of certain elements that are very rare on the Moon, such as H, C, N, and the noble-gas elements (see section 8.8).

Solar cosmic rays. Most particles in the solar cosmic rays are stopped by ionization energy losses in the top few centimeters of the lunar surface. The heavy nuclei in the SCR are rapidly stopped in the outer millimeter of the Moon and can produce high densities of radiation damage there (*Walker,* 1975*; Reedy et al.,* 1983). Solar proton fluxes, especially those at lower energies, drop rapidly with depth in the Moon because of the slowing down of these fairly low energy particles (*Reedy and Arnold,* 1972). The few reactions induced by SCR particles are mainly in the top centimeter of the lunar surface, and few secondary particles are emitted in these reactions. Over many years, the average flux of secondaries from SCR particles is much less than those from GCR particles (*Armstrong and Alsmiller,* 1971), although the flux of secondaries in the top ~100 g/cm^2 of the Moon could be relatively high during the peak of an intense, hard SCR event. The relatively small cascade of particles induced by SCR particles does not penetrate deeply.

Galactic cosmic rays. The heavy nuclei in the galactic cosmic rays are usually stopped by ionization energy losses within ~10 cm of the lunar surface. Most of the radiation damage induced by these heavy GCR nuclei occurs within the top few centimeters. This radiation damage is so intense that it can be seen as high densities of tracks in lunar samples (*Walker,* 1975; *Reedy et al.,* 1983) and can cause problems in sensitive electronic components (*Adams and Shapiro,* 1985). Shielding of a few g/cm^2 is usually adequate to remove most of these highly-ionizing heavy GCR nuclei.

The lighter nuclei in the GCR, mainly protons and alpha particles, are very penetrating and induce a cascade of particles that extends meters into the lunar surface. The number of secondary particles in this GCR cascade is much greater than the number of incident primaries. For example, the flux of GCR primary particles hitting the lunar surface is about two particles/cm^2 sec, while the number of secondary neutrons made in the lunar surface is about 13

neutrons/cm^2 sec (*Reedy et al., 1983*). Additional secondary particles, such as pions, are also present in this cascade (*Armstrong and Alsmiller,* 1971), although the dominant particle in the cascade is the neutron (mainly because neutrons are not slowed by ionization energy losses). For energies below ~100 MeV, most particles in the Moon are neutrons (*Armstrong and Alsmiller,* 1971; *Reedy and Arnold,* 1972). These neutrons are typically produced with energies of a few MeV and travel through the Moon until they interact (most effectively with elements lighter than oxygen) or escape into space (*Lingenfelter et al.,* 1961, 1972). *As* elements lighter than oxygen are very rare in the Moon, neutrons lose energy slowly and many collisions are required to degrade the energy of a neutron to near thermal (below ~0.1 eV) energies (*Lingenfelter et al.,* 1961, 1972).

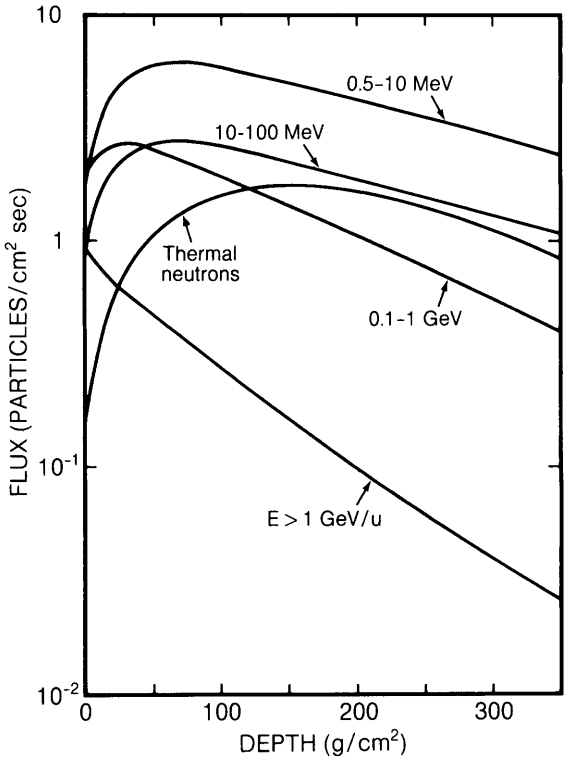

Fig. 3.20. Fluxes of galactic-cosmic-ray particles, both incident primaries and secondaries, as a function of depth in the Moon (a depth of 350 g/cm^2 is about 2 m of lunar regolith). Profiles were calculated with the lunar-GCR-particle model of *Reedy and Arnold* (1972), except for the thermal neutron profile (from *Lingenfelter et al.,* 1972). High-energy (>1 GeV/u) particles are removed rapidly with increasing depth while lower-energy particles first increase but eventually decrease with depth. For doses vs. depth in the Moon, see *Silberberg et al.* (1985) or *Letaw et al.* (1987).

Galactic-cosmic-ray particle fluxes, both the incident primaries and the secondaries, are shown in Fig. 3.20 as a function of depth in the Moon for several energy groups. *Armstrong and Alsmiller* (1971) give a plot of the fluxes of neutrons for eight energy groups. The particles with energies above 1 GeV/u are mainly the primary nuclei and some high-energy secondaries (*Reedy and Arnold,* 1972). The particles below ~100 MeV/u are mainly secondary neutrons, and the particles between 100 MeV/u and 1 GeV/u are a mixture of primaries and secondaries, although secondaries usually dominate, especially at greater depths in the Moon. The curves in Fig. 3.20 are based on the model of *Reedy and Arnold* (1972) for energies above 0.5 MeV and the neutron-transport calculations of *Lingenfelter et al.* (1972) for thermal neutrons. The fluxes of high-energy particles decrease almost immediately below the lunar surface because these particles are removed from the primary GCR by attenuation. The lower-energy secondaries have flux-vs.-depth profiles that reflect both their buildup and subsequent attenuation. The deep peak for the thermal neutrons is largely due to the fact that many neutrons near the surface escape from the Moon before they can be slowed to thermal energies.

3.11.5. Implications of the Lunar Radiation Environment

Scientific studies. The products of the interactions of the solar wind, the solar cosmic rays, and the galactic cosmic rays with the Moon have been used for a large variety of scientific studies (*Reedy et al.,* 1983; *Walker,* 1975). The solar wind and cosmic ray records of lunar materials have been investigated in detail. These studies, which determine how these radiations interacted with lunar samples, have provided records of the histories of both the radiation and the lunar samples themselves. The results of some of these investigations will only be briefly discussed here (see *Reedy et al.,* 1983, *Walker,* 1975, and references therein for additional details).

As mentioned above, lunar samples have provided a good record of solar wind and SCR particles in the past. It is largely based on the lunar record for SCR particles over the past ~10^7 years that we can make many of the statements in section 3.11.2 about the SCR particle fluxes expected at the lunar surface. The amounts of the products from solar wind, SCR, or GCR interactions can be used to determine the length of time that a lunar sample was within

micrometers, centimeters, or meters, respectively, of the lunar surface. Such "exposure ages" cover a wide range, from material freshly ejected from craters to pieces of the regolith that have been near the surface for ~1 b.y.

These exposure ages have been used to help date a number of lunar features, such as craters. Profiles of cosmic-ray-produced nuclides have been used to determine the rate that the regolith has been disturbed by impacts (see *Reedy et al.,* 1983). The top few centimeters of the regolith have been mixed on timescales of a few millions of years. The deepest parts of the ~2-m-long cores brought back from the Moon usually have been disturbed on much longer timescales. Most rocks have been on the lunar surface for much less than 1 b.y., and usually have been knocked around on timescales of ~10 m.y. Very old rocks are extremely rare because rocks on the lunar surface eventually are destroyed or deeply buried by impact processes.

Another use of the lunar radiation environment has been the study of gamma rays and neutrons emitted as the result of the interaction of GCR particles in the lunar surface. Some of these gamma rays and neutrons subsequently escape into space. Many of the gamma rays have energies that uniquely depend on the nuclide from which they were produced (*Reedy,* 1978). By measuring the gamma rays above the lunar surface, the elemental composition of the top layers of that surface can be determined. This was the basis of the Apollo orbiting gamma-ray spectrometer, which provided useful chemical maps of Th, Ti, Fe, Mg, and K (see section 10.2.2). The neutrons leaking from the lunar surface are also sensitive to the surface chemical composition, especially its hydrogen content (*Lingenfelter et al.,* 1961); detection of neutrons could be used as an exploration tool for near-surface hydrogen or water (especially at the lunar poles; see section 3.8).

Radiation effects in the Moon. Each of the three radiation types in the lunar environment produces its own set of effects. The solar wind can produce sputtering and amorphous material in the very outermost layers (<1 μm) of the particles on the lunar surface and many of these ions become implanted. Lunar grains with these near-surface solar-wind effects usually become buried deeper by impact debris.

The solar cosmic rays typically interact with the top millimeter to top few centimeters of the lunar surface, mainly by ionization energy loss. The heavy SCR nuclei can induce locally high doses near the end of their ranges. Solar-cosmic-ray events occur irregularly, mainly at times when the sun is relatively active, and the dose rates from SCR particles range from nothing to very high levels for several hours during rare, very intense events (*Rust,* 1982; *Letaw et al.,* 1987). These rare, very intense SCR events are potentially the greatest radiation hazard on the Moon; it is difficult to predict their occurrence and severity.

The GCR particles are the most penetrating of the radiation types but also are very predictable. The heavy nuclei in the GCR typically penetrate only a few centimeters, but the cascade of secondary particles, especially neutrons, made by the GCR protons and alpha particles penetrates meters into the Moon. Fairly high radiation doses result from these GCR particles (*Silberberg et al.,* 1985). The incident fluxes of GCR particles vary by about a factor of 2 over a typical 11-year solar cycle and are expected to be most intense during solar minima. During rare (every ~200 years), long periods of low solar activity (like the Maunder Minimum), the fluxes of GCR particles could be up by a factor of ~3 when compared with a typical solar minimum.

Summary. The radiation that hits the Moon is very diverse. It includes huge fluxes of ~1 keV/u solar-wind ions, a few high-energy (>1 GeV) GCR particles, and high-energy SCR particles intermittently emitted from the sun. The radiations at the lunar surface are very different from those on the Earth because the Moon lacks both a strong magnetic field and a thick atmosphere.

At the lunar surface, this radiation produces distinct, permanent, and depth-dependent effects. These effects, studied in lunar samples, have been used for a number of valuable scientific studies that include dating the ages of lunar features, determining the rate of "gardening" of the lunar regolith by meteoroids, and establishing a historical record for the past behavior of the sun.

The energies and fluxes of the particles hitting the Moon span many orders of magnitude (Table 3.5). Furthermore, their compositions differ and can vary with time and energy. Their lunar penetration depths vary from less than a micrometer to several meters. The solar-wind ions are implanted in the very surfaces of grains on the lunar surface, and these solar particles are the main source of certain volatile elements in the lunar regolith. The heavy nuclei in the galactic cosmic rays and the many secondary particles, especially neutrons, that the GCR generate in the lunar soil require the use of shielding to protect humans and sensitive electronic equipment on the Moon. Energetic particles from the sun are generally a minor concern on the Moon, but a few very large solar particle events, produced by flares, can occur each decade. These events would be very serious radiation hazards for humans and equipment exposed on the lunar surface.

APPENDIX

A3.1. Motion of the Earth-Moon System

Viewed from above the north pole of the Earth, the Moon travels counterclockwise in a slightly elliptical path around the Earth. At closest approach (perigee) the Moon is 356,410 km from the Earth and at farthest distance (apogee) it is 406,697 km away. From the Earth the apparent diameter of the lunar disk varies systematically with these changes in distance (*Glasstone,* 1965; *Mutch,* 1970).

The average period of revolution of the Moon about the Earth, using the stars as fixed reference points, is 27.322 days or *a sidereal month* (Fig. A3.1). Because of the gravitational effects of the sun on the Moon, the period of revolution varies from one revolution to the next; variation from the mean value can be several hours. The *synodic month is* the time

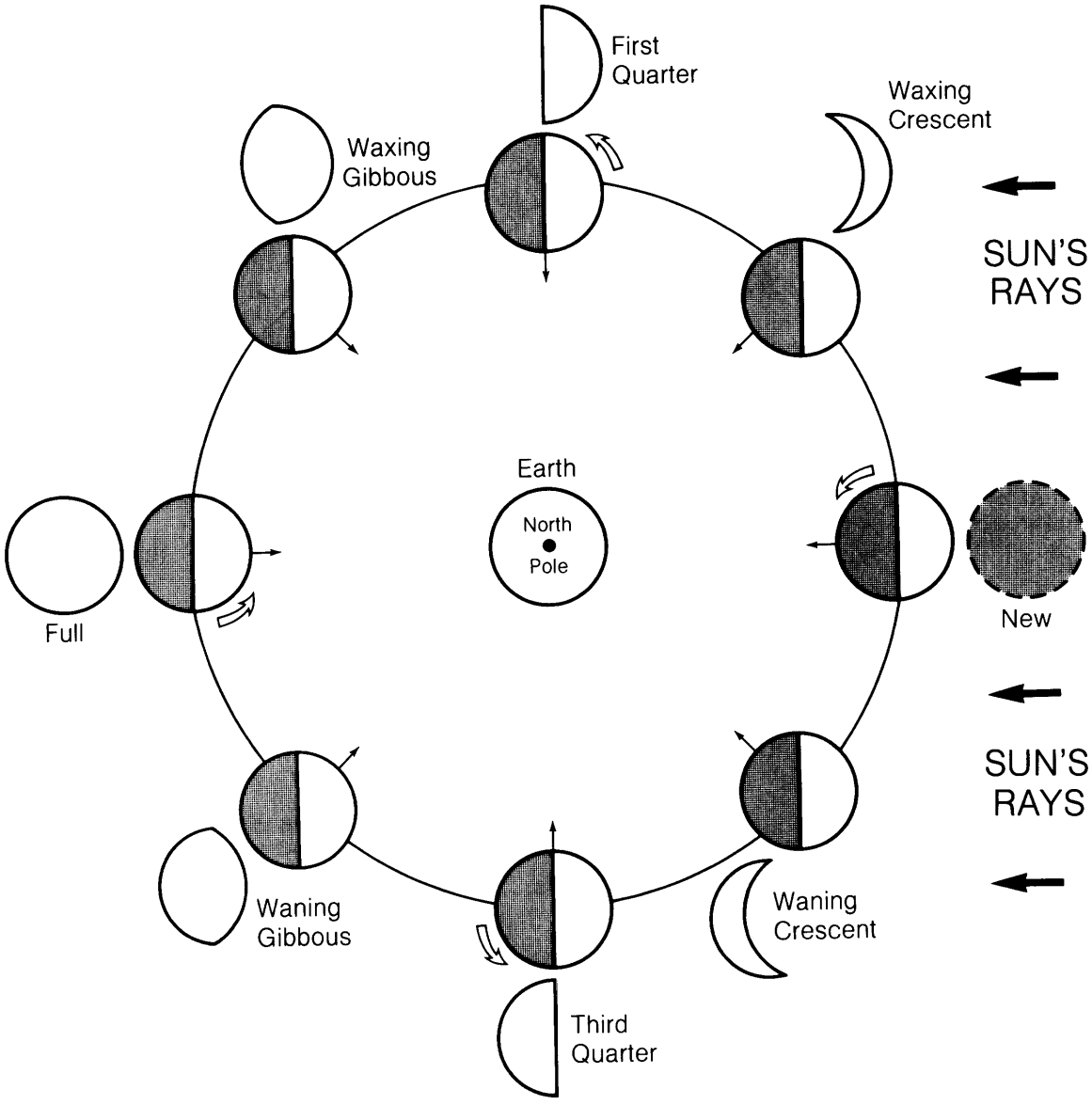

Fig. A3.1. Revolution of the Moon around the Earth, showing the combination of its orbital motions with its gravitationally "locked" rotation that causes it to present only one face to the Earth (from *Mutch,* 1970).

between two successive alignments of the Moon with the sun, observed from the Earth; this is also the time between successive new Moons and is called the *lunar month* (Fig. A3.1). The observed average lunar month is 29.531 days; variation from this value can be up to 13 hours.

The geometry of the Moon's rotation about its axis and orbit around the Earth is shown in Fig. A3.2. The periods of rotation and revolution are virtually identical, with a fixed lunar *nearside* that faces the Earth and *a farside* that faces away (Fig. A3.1). The relative motions and orientations of the Earth and Moon (Figs. A3.3 and A3.4), however, do allow the Earthbound observer to see slightly more than half of the lunar surface because of *librations* in both longitude and latitude.

Longitudinal libration, caused by the slight non-circularity of the Moon's orbit, is an apparent rocking back-and-forth motion of the Moon in an east-west direction (Fig. A3.3). Because of this libration, it is possible to see an additional 7.7° along both eastern and western limbs of the lunar disc (*Glasstone,* 1965). *Latitudinal libration is* caused by the inclination of 6.7° of the Moon's axis of rotation to a line

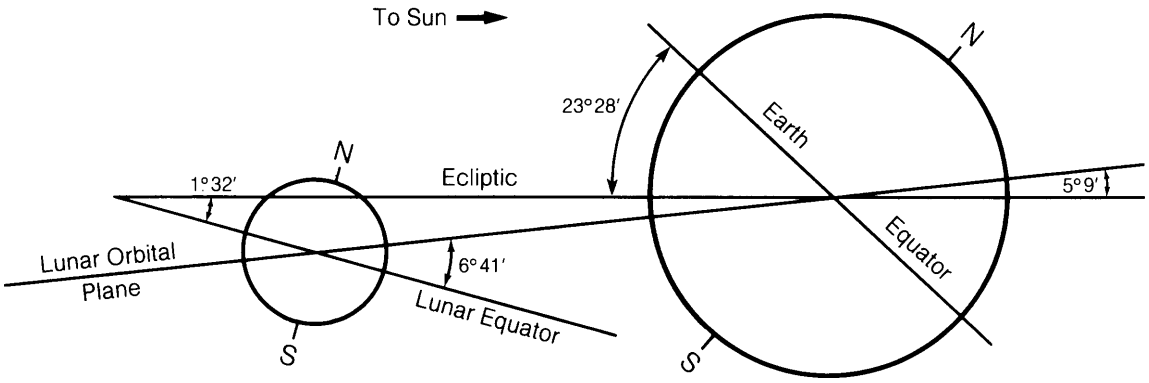

Fig. A3.2. Geometric relationship between the planes of revolution and rotation in the Earth-Moon system. Note that angular relationships have been exaggerated (from *Mutch,* 1970).

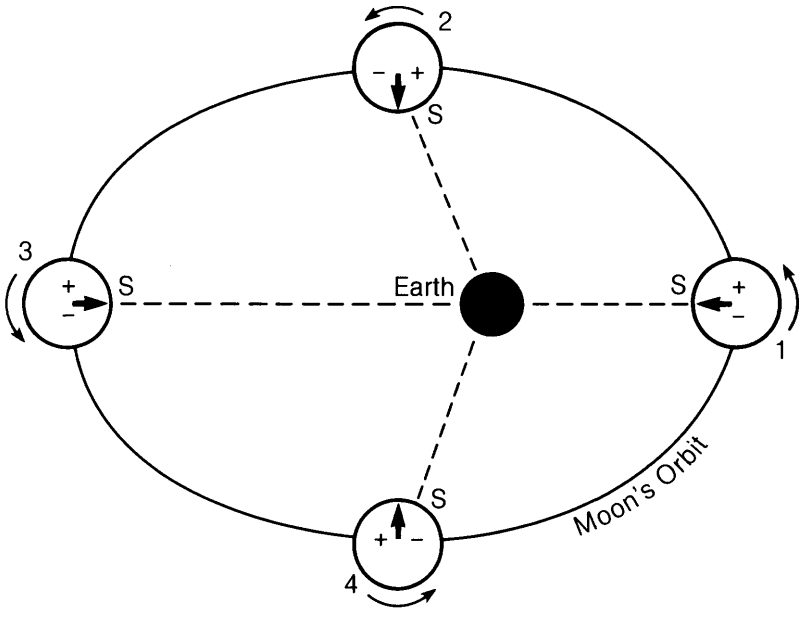

Fig. A3.3. Illustration of longitudinal libration. Because of the elliptical orbit of the Moon, positions 2 and 4 present slightly displaced subterrestrial viewpoints(s); this libration is positive (to the right of the arrow that marks the lunar prime meridian) at point 2 and negative (to the left of the lunar prime meridian) at point 4. The net result is that we see slightly more of the Moon's near-equatorial surface than we otherwise would from Earth (from *Mutch, 1970*).

perpendicular to the lunar orbital plane (Fig. A3.4). Because of this, it is possible to see an additional 6.7° at the north and south poles, over two-week intervals.

The *diurnal libration is* a parallax effect caused by rotation of the Earth. The position of an observer on the Earth's equator will move laterally about 13,000 km during a 12-hr period. This gives a libration of 1° at the western edge of the Moon upon rising and 1° at the eastern edge when it sets.

Because of these combined librations, we can see about 60% of the lunar surface from the Earth.

A3.2. Brightness of the Lunar Surface

Brightness of any spot on the Moon is dependent upon *phase angle, brightness longitude,* and *albedo* of the rocks or regolith. *Phase angle is* the angle measured between incident solar radiation and the emergent ray as seen by the observer (see Fig. 3.1). *Brightness longitude is* "the angle measured in the plane between the emergent ray and a line perpendicular to the intersection of the ground with the phase plane" (*Mutch,* 1970).

Albedo is the fraction of visible electromagnetic radiation reflected by the surface of a material. Overall, in visible light, the Moon is a dark object with albedos ranging from about 7% to 24%. The light-colored rocks of the lunar highlands have variable but generally high albedos (mostly about 11% to 18%) whereas the basaltic lavas of the lunar maria have low albedos (about 7% to 10%). Earth-based albedo measurements are made during full Moon.

Brightness varies systematically with changing phase angle, so that total lunar brightness is lower than the fraction of the lunar surface illuminated

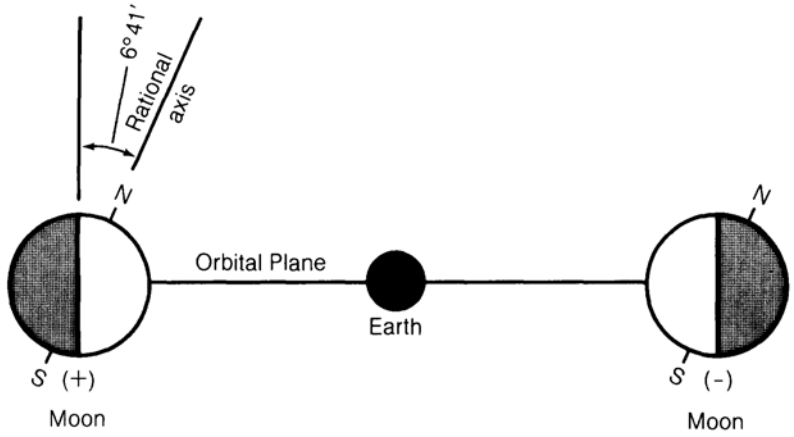

Fig. A3.4. Illustration of latitudinal libration (from *Mutch,* 1970). Views of the north polar region result from positive latitudinal libration; views of the south polar region result from negative latitudinal libration. The net result is that we see more of the Moon's polar regions than we otherwise would from Earth.

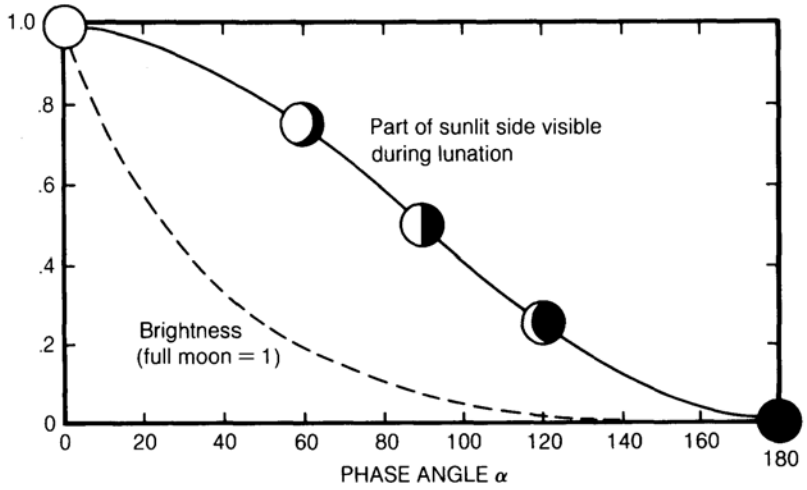

Fig. A3.5. Variation of total lunar brightness detected at Earth (scale of 0 to 1.0, dashed curve) compared with the fraction of the lunar surface visible from Earth (also on a scale of 0 to 1.0, solid curve with lunar images). Brightness decreases more rapidly than the fraction of surface illuminated as the Moon wanes, and increases more slowly as the Moon waxes (after *Mutch, 1970*).

(Fig. A3.5). For a review of photometric studies of the lunar surface and lunar materials, see *Wilson* (1971).

A3.3. Locating Points on The Moon

Selenodesy, or mapping of the Moon, began with Aristotle (384-322 B.C.) and has continued to today, building on the work of such famous astronomers as Galileo (1610), Langrenus (1645), Cassini (1680), Schroter (1791), and many others. Beginning in 1959, the U.S. Air Force Aeronautical Chart and Information Center (ACIC) began an international cooperative project to map the Moon's nearside at a scale of 1:1,000,000; 44 individual maps were prepared and completed in 1967. All of this work was based upon Earth-based telescopic photographs.

As a result of the Lunar Orbiter flights of 1966-1967, most of the Moon was photographed. How-ever, because of photographic distortions, few of these images have been used for cartography other than general mapping of surface features. Mapping cameras (panoramic and metric) carried on the last three Apollo missions were used to produce topographic maps of a near-equatorial band around the Moon below the command module flight paths. For a complete review of lunar mapping, see the Lunar Cartographic Dossier by *Schimerman* (1973).

Lunar maps have followed Earth convention since 1961, with north at the top and the prime meridian referenced to Crater Mosting A on the Moon's nearside. Before 1974, maps expressed lunar longitude in terms of 0° -180° east (+) and 0° -180° west (-) of the prime meridian; this convention is used in this book. After 1974, a lunar longitude system of 360°, proceeding counterclockwise (increasing to the east) from the prime meridian, was adopted by international agreement for future cartography.

The names of lunar features varied from map to map until 1907 when a committee of the International Association of Academies was appointed to bring some uniformity to the problem; a collated list was published in 1913. Eventually the International Astronomical Union took on the responsibility of naming lunar features and keeping track of nomenclature. The following resolution was made:

> "For designating the lunar surface features, it is recommended to follow the previous rules, revised and improved as follows: (i) Craters and rings or walled plains are designated by the name of an astronomer or prominent scientist deceased, written in the Latin alphabet, and spelled according to the recommendation by the country of origin of the scientist named. (ii) Mountain-like chains are designated in Latin by denominations allied with our terrestrial geography. Names are associated with the substantive Mons according to the Latin declension rules and spelling. (Three exceptions, Montes d'Alembert, Montes Harbinger, and Montes Leibnitz are preserved, due to former long use).
> (iii) Large dark areas are designated in Latin denominations calling up psychic states of mind. These names are associated, according to the Latin declension rules and spellings, to one of the appropriate substantives Oceanus, Mare, Lacus, Palus, or Sinus. (The exceptions Mare Humboldtianum and Mare Smythii are preserved, due to former long use).
> (iv) Isolated peaks are designated according to the same rules as for the craters, as well as promontories, the latter being preceded by the Latin substantive Promontorium. (v) Rifts and valleys take the name of the nearest designated crater, preceded by the Latin substantives Rima and Vallis (The exception Vallis Schroter is preserved). (vi) Undenominated features can be designated by their coordinates. They can equally be designated according to the former classical system, by taking the name of the nearest crater, followed by a block letter of the Latin alphabet for craters, depressions and valleys, by a minor letter of the Greek alphabet for hills, elevations and peaks, and by a Roman number followed by the letter r for the clefts."

At an IAU Assembly in 1973, the surface of the Moon was divided into 144 named regions at a scale of 1:1,000,000, by means of parallels of latitude and meridian arcs. It was also resolved to drop Greek letter designations for lunar elevations and crater names by use of a Roman capital letter. Ridges will be called *dorsa* and crater chains designated *catena.* Future name assignments will also contain the names of distinguished and deceased contributors to human culture and knowledge; political, military, and religious figures were excluded. Maps with all lunar names are too large for this sourcebook.

The reader is referred to The Rectified Lunar Atlas (*Whitaker et al.,* 1964; *Wilhelms,* 1987) for more details.